VARIABILITY OF GROUND HEAT FLUX AT TIKSI STATION

by

SARA M. MORRIS

B.A., University of Colorado, 2010

A thesis submitted to the

Faculty of the Graduate School of the

University of Colorado in partial fulfillment

of the requirement for the degree of

Master of Arts

Department of Geography

2018

This thesis entitled:
Variability of Ground Heat Flux at Tiksi Station
written by Sara Marie Morris
has been approved for the Department of Geography

____
Dr. Mark Serreze (Committee Chair)

____
Dr. Ola Persson (Committee Member)

Date ______________

The final copy of this thesis has been examined by the signatories, and we find that both the content and the form meet acceptable presentation standards of scholarly work in the above mentioned discipline.

Abstract

Morris, Sara Marie (M.A., Geography Department)

Variability of Ground Heat Flux at Tiksi Station

Thesis directed by Professor Mark Serreze

This study examines the spatial variability in ground heat flux measured at four sites in the vicinity of the Russian Arctic meteorological observatory at Tiksi during a full annual cycle in 2016. Nine land cover types were identified surrounding the Tiksi observatory using a map acquired from World View via the Finnish Meteorological Institute (FMI). FMI found that land cover types vary in the vicinity of the observatory on scales of meters, implying that this information needs to be taken into account to properly upscale point measurements for comparisons to models. The ground heat flux was calculated using flux plates and soil temperature measurements at four identified soil locations: stony, grassy (two flux plates at this location), dry fen, and wet fen. To obtain a ground heat flux value, a term is also included to account for changes in energy stored in the soil above the measured ground heat flux plate at each of the measurement sites. This change in energy storage was estimated from measured temperature profiles and soil heat capacities from published studies. Results highlight the difficulty in defining soil properties necessary for calculating the storage change and of obtaining direct flux measurements from all land cover types in an Arctic region.

Results also demonstrate the need for weighted averages of ground heat fluxes to upscale to model or satellite grid scales.

Dedication

The challenge to identify a research topic in the Arctic was surprisingly easy. The difficulty came later in understanding the level of detail necessary to collect quality data for my research in the harsh environment of the Arctic. Details such as data continuity, instrument functionality, and data availability were all challenges I encountered when trying to consolidate a reasonable data set from not only the Arctic field project, but from the international Arctic community. Through these challenges I was lucky to have the guidance from my NOAA science supervisor, Taneil Uttal, who taught me to not bat an eye at any one of these challenges, no matter how impossible they might seem. Taneil not only pushed me to become a better researcher, but she taught me how to navigate the waters of international communication in the Arctic across a multitude of communities. Dr. Mark Serreze supported my initiative to become a graduate student while also continuing to work full-time at NOAA. Mark taught me how to think "big picture" when it came to navigating Arctic science, while never compromising on the details that make up solid research. Above all I would like to dedicate this thesis to my support behind the scenes, my husband Drew, and my family and friends, who never hesitated to lift me up when the project seemed to overwhelming to complete. Finally, I dedicate this thesis to the next generation of scientists – may you never lose sight of the importance of research.

Acknowledgements

I acknowledge the station technicians and staff at Tiksi for continuing to support the mission of data collection in one of the harshest environments of the world. I also acknowledge the National Oceanic and Atmospheric Administration (Physical Sciences Division), the Cooperative Institute for Research in Environmental Sciences, the Finnish Meteorological Institute, the Russian Federal Services for Hydrometeorology and Environmental Monitoring, and the Arctic and Antarctic Research Institute. Thanks to Mika Aurela and Thomas Laurila for their support in providing the Tiksi soil maps and categories. Thanks to Elena Akish for programming support, and to Christopher Cox for programming and analytical support. Thanks also to Andrey Grachev, Ola Persson, and Peter Blanken for their contributions and their motivation to continue research in this field.

Contents

List of Tables

Table 11. Comparisons between results from flux plates (G) at each the GrassyA and Grassy B locations to evaluate how the instruments compare to one another. This comparison is most useful when instruments are co-located, so the results from the comparison of GrassyA and GrassyB are most accurate (compared to the other sub-station instruments) to determine instrument biases. Error was determined by instrument specifications, while biases were determined by instrument comparison. The RMS difference was smaller than the annual mean.

List of Figures

1. Introduction

One of the fundamental impacts on Arctic climate is the exchange of energy between the atmosphere and the ground surface (Serreze & Barry, 2005; Westermann, Luers, Langer, Piel, & Boike, 2009). Few direct measurements of the full surface energy budget exist in the Arctic, and information on the ground heat flux is especially sparse. Measurements of the ground heat flux at locations such as the Tiksi Observatory (Uttal, 2013) in Tiksi, Russia, are hence extremely valuable, especially given concerns about warming permafrost and changes in the active layer (Boike, Roth, & Ippisch, 2003; Serreze & Barry, 2005; Westermann et al., 2009). Key challenges in understanding Arctic ground heat fluxes are that (1) it is difficult to obtain accurate measurements, and (2) values are likely to vary strongly across the landscape due to differences in soil properties, slope, aspect and other factors. This study, which examines the ground heat flux at four sites around Tiksi observatory, is designed to address these key challenges.

Closing the surface energy budget based on directly measured terms is always challenging, but it is especially difficult in the harsh Arctic environment where infrastructure and site support is typically limited (Foken, 2008). In assessing the degree of closure, it is critical to examine the methods by which each individual flux (i.e. radiative flux, turbulent flux, and ground heat flux) is obtained. Deriving a ground heat flux can be difficult in Arctic regions where homogeneous landscapes are rare; especially, in coastal regions where the active layer can vary greatly in soil moisture content (Hinzman, Kane, Gieck, & Everett, 1991).

This study investigates the best methods for capturing a more complete representation of ground heat flux for the Tiksi observatory. The observatory established an international partnership that led to the building of a meteorological station, a clean air facility, and a flux tower on-site in 2010. Tiksi was designated as an ideal Arctic station location due to its historical weather station dating back to 1932, and its coastal location in Russia where measurements have been limited. The location of Tiksi prompted international collaborations to facilitate other infrastructures focused on measuring atmosphere-surface exchanges, and aerosol and solar radiation measurements. The NOAA-Physical Sciences Division, in collaboration with the Arctic and Antarctic Scientific Research Institute (AARI) and the Finnish Meteorological Institute (FMI), has developed a local network of sensors at the Tiksi observatory, enabling the ground heat flux and its variability to be assessed at four locations to understand the impact of different land cover types. While at most Arctic stations, including Tiksi, soil parameters (thermal conductivity and heat capacity) are not directly measured, such information is critical for calculating a ground heat flux. This study hence also seeks to address the implications for ground heat flux estimates where soil parameters are not directly measured.

1.1 Motivation: Surface Energy Budget

The ground heat flux is a key part of the surface energy budget:

$$Q^* = Q_E + Q_H + Q_G \tag{1}$$

Where Q^* is the net radiation flux, Q_E is the latent heat flux, Q_H is the sensible heat flux, and Q_G is the adjusted ground heat flux (Foken, 2008; Persson, Fairall, Andreas, Guest, & Perovich, 2002). The convention is written so that radiation terms (included in the net radiation) are defined as positive downward toward the surface and non-radiative terms are defined as positive away from the surface. Terms on the right (assuming no snowmelt) should theoretically balance with the net radiation term (Foken, 2008; Halliwell, Rouse, & Weick, 1991; Heusinkveld, Jacobs, Holtslag, & Berkowicz, 2004; Hinzman, Goering, & Kane, 1998; Persson et al., 2002). Historically, the ground heat flux term has been given less attention than the other terms due to its relatively smaller values. However in the Arctic, it is an important term to assess trends of warming in the active and permafrost layers.

The adjusted ground heat flux term (Q_G) fluctuates throughout the seasons, but is generally positive (away from the surface) during summer and negative (toward the surface) in winter. This is expected as incoming shortwave radiative fluxes (Q_{SW}) warm the surface in summer and outgoing longwave fluxes cool the surface (Q_{LW}) in winter while the sun is down. The summer influx of energy to the soil is seen in the thawing of the active layer, where the temperature gradient of the soil becomes warmer at shallow depths near the surface and cooler down below near the permafrost layer. In the absence of incoming solar radiation during winter we see a shift in the soil temperature gradient, where the soil temperature now becomes cooler at shallow depths and warmer further down. In winter when a snow pack has developed on top of the soil, we can expect the snow pack to act as an insulating layer where the base of the snow pack becomes warmer than the top. Figure 1 is a schematic of the surface energy budget in the Arctic.

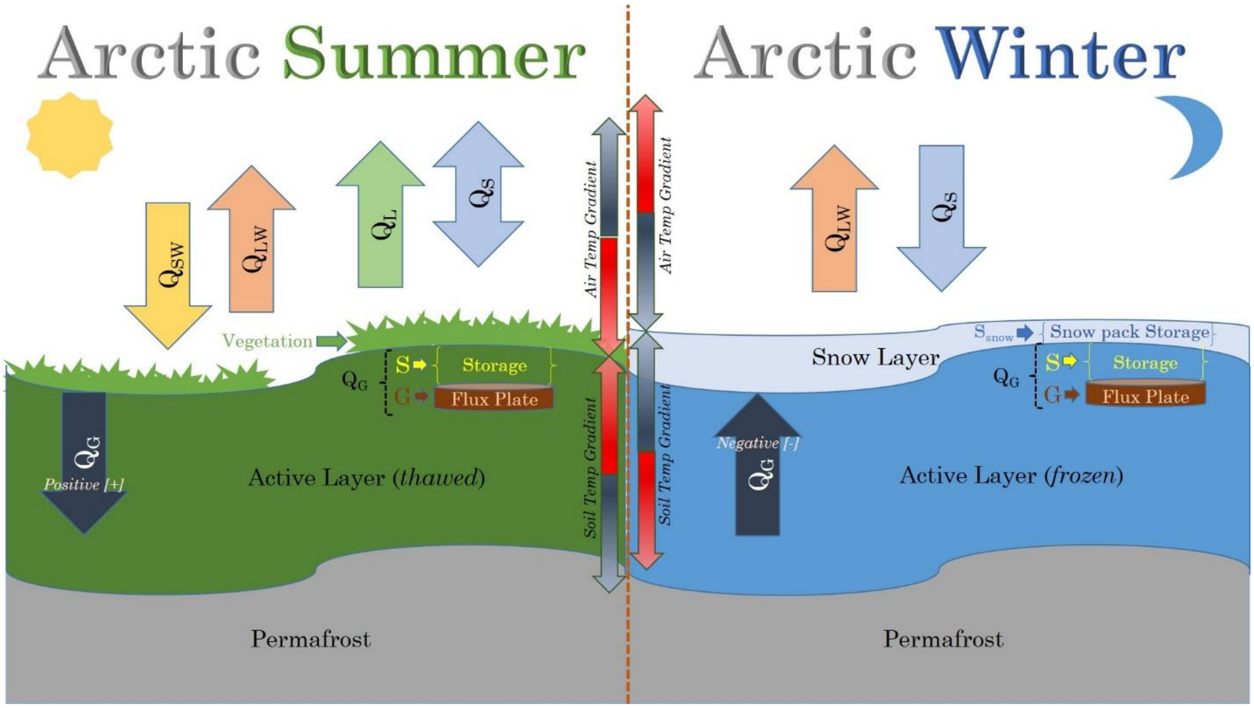

Figure 1. Conceptual schematic of the generalized terms within the surface energy budget in the Arctic during summer and winter seasons. Q^* = net radiation flux (comprised of Q_{SW} = shortwave flux and Q_{LW} longwave flux), Q_G = adjusted ground heat flux, Q_L = latent heat flux, Q_H = sensible heat flux. The flux arrows in summer will vary directionally with the diurnal cycle. All arrow sizes are identical in magnitude as the schematic is meant to illustrate the contributing sources to the surface energy budget and ground heat flux equations.

Referencing Figure 1, the ground heat flux (G) is defined as the rate of thermal energy (W m^{-2}) flowing through a specified level in the ground (or active layer, for the purposes of this research). The ground heat flux can be measured directly from a flux plate or from soil temperature probes by measuring temperature gradients in a layer of soil with respect to depth and time (Liebethal, Huwe, & Foken, 2005). Since the surface energy budget references the interface between the surface and atmosphere, and in practice the ground heat flux (G) is measured at some depth below the surface, it is necessary to account for any changes in energy stored in the soil above the flux plate measurement level. This is considered the storage change term (S), and is calculated from the storage layer temperature gradient and known soil variables (soil heat capacity and thermal conductivity). The summation of both the measured ground heat flux (G) and the storage change term (S) make up the adjusted ground heat flux (Q_G). The generic equation is (Halliwell & Rouse, 1987; Liebethal et al., 2005; Peters-Lidard, Blackburn, Liang, & Wood, 1998; Philip, 1961):

$$Q_G = G + S \tag{2}$$

Where $\boldsymbol{Q_G}$ is the adjusted ground heat flux [units = Wm^{-2}], $\boldsymbol{G}$ is the derived or measured flux value at instrument depth [units = Wm^{-2}], and $\boldsymbol{S}$ is the flux storage change term. This storage change term [units = Wm^{-2}] is derived from changes in temperature (ΔT) and depth (z) with respect to time (Δt) as measured from corresponding instrumentation (the term includes a derived soil heat capacity (C_{psl}) value for the designated land cover type).

$$C_{psl} = \rho_a c_a \theta_a + \rho_s c_s \theta_s + \rho_w c_w \theta_w \tag{3}$$

Where $\mathbf{C_{psl}}$ is the soil heat capacity, $\boldsymbol{\rho}$ is the bulk density of air (ρ_a), solid (ρ_s), or water (ρ_w), $\mathbf{c}$ is the specific heat of air (c_a), solid (c_s), or water (c_w), and $\boldsymbol{\theta}$ is the volumetric content of air (θ_a), solid (θ_s), or water (θ_w). Incorporating the soil heat capacity, the storage change term can be expanded as:

$$\boldsymbol{S} = \frac{\Delta T * C_{psl} * z}{\Delta t} = \frac{\left(\left(T_{05}^{n+1} - T_{05}^{n-1} + T_{sfc}^{n+1} - T_{sfc}^{n-1}\right) * C_{psl} * z\right)}{2(t_{n+1} - t_{n-1})} \tag{4}$$

Depending on the instrument type used and the data collection methods available, thermistor probes may also be used to derive a ground heat flux value, $\boldsymbol{Q_G}$, (instead of flux plates). The measured ground heat flux value, $\boldsymbol{Q_G}$, would then be expanded to:

$$Q_G = -K_{sl}\frac{\Delta T}{\Delta z} - C_{psl}\frac{\Delta T}{\Delta t}\Delta z \tag{5}$$

Where $\boldsymbol{K_{sl}}$ is the soil thermal conductivity [units = $Wm^{-1}K^{-1}$], and $\boldsymbol{C_{psl}}$ is the soil heat capacity [units = $Jm^{-3}K^{-1}$].

The soil properties that affect the ground heat flux, specifically soil thermal conductivity and soil heat capacity, are highly soil dependent, meaning that it is advantageous to measure these soil properties when also measuring the flux (Foken, 2008; Heusinkveld et al., 2004; Peters-Lidard et al., 1998). Soil thermal conductivity is not represented in the ground heat flux calculation when using the flux plate instrument method – the thermal conductivity constant is instead represented in the calibration coefficient of the flux plate itself. This is due to the temperature gradient being measured across a known conductivity substance of the plate's material instead of through the soil (Hukseflux, 2015). By contrast, fluxes measured from the thermistor probes must include a thermal conductivity value since the temperature probe simply measures a temperature gradient across the soil (Halliwell & Rouse, 1987; Hinzman et al., 1998; Kane, Hinkel, Goering, Hinzman, & Outcalt, 2001; Romanovsky & Osterkamp, 1997). Additionally, soil thermal conductivity is strongly correlated to both the amount and phase of water (solid versus liquid), which can vary in the active layer. This is important as it will determine which soil constants should be used at specific times of year (i.e. ice and water will conduct thermal energy differently through the soil).

2. Background

2.1 State of the Field: Ground Heat Flux

When measuring ground heat flux, it is important to understand errors introduced throughout the data collection and processing steps, and to clarify how ground heat fluxes vary across landscapes. Specifically, applications of this study relate strongly to how errors in the ground heat flux term can influence the total surface energy budget in the Arctic. The broader implications include defining how to obtain the best-possible ground heat flux measurements, and how that measurement might change across landscapes in the Arctic. As such, it is imperative to assess previous results and outcomes.

A major challenge is determining whether or not a single-site observation is enough to capture the spatial variability in ground heat flux. Since the flux is determined from a series of observations and strategies (i.e. flux plate measurements, skin temperature measurements, soil depth temperature measurements, soil heat capacity observations, soil thermal conductivity observations), it is imperative to investigate how other studies have addressed issues with quantifying ground heat flux for an entire region. By analyzing the state of the field of ground heat flux measurements in different land cover types and locations, one can assess the difficulties in deriving a ground heat flux term with enough accuracy for the surface energy budget (Hinzman et al., 1991; Romanovsky & Osterkamp, 1997; Watanabe, Kiyosawa, Fukumura, Ezaki, & Mizoguchi, 2003).

It is recognized that the soil heat capacity and thermal conductivity are important in deriving the flux for a given temperature gradient within the soil, and that analyses of soil properties in parallel to ground heat flux measurements is common (Halliwell et al., 1991; Peters-Lidard et al., 1998; Romanovsky & Osterkamp, 1997). With water content being a factor in energy storage in soils, thereby impacting ground heat flux, accurately measuring the soil water content is also imperative in Arctic regions where permafrost is abundant (Eaton, Rouse, Lafleur, Marsh, & Blanken, 2001; Peters-Lidard et al., 1998). Previous research has found that the depth of the active layer is important and is linked to variations in the ground or surface temperatures and water content (Romanovsky & Osterkamp, 1997). Some studies attempted to model the thermal distribution (Hinzman et al., 1998), while others derived algorithms to assimilate the soil properties such as porosity, water content, and soil temperature to determine whether soils were frozen or thawed (Nicolsky, Romanovsky, & Panteleev, 2009).

Other investigations have concluded that knowledge of soil properties are important in deriving the ground heat flux of an area, and that whether or not soils are frozen or thawed can dramatically change the magnitude of the ground heat flux (Evett, Agam, Kustas, Colaizzi, & Schwartz, 2012; Hinkel, 1997; Watanabe et al., 2003). Hinkel (1997) also addressed issues with temporal lag as heat permeates through different land cover types at different rates, thereby impacting the time collection methods of ground heat flux measurements (Kane et al., 2001).

Ground heat flux measurements using flux plates, as described above, should also be accompanied by a term that captures the change in energy stored (S) in the layer of soil directly above the plate (Liebethal et al., 2005; Meyers & Hollinger, 2004). This term is dependent on soil properties and soil moisture content that can vary with frozen and thawed land cover types, as described previously (Kane et al., 2001; Nicolsky et al., 2009; Oliphant et al., 2004). Traditionally, the storage change term referenced in the derivation of ground heat flux is defined in terms of the heat energy stored in the soil directly above the buried flux plate (Heusinkveld et al., 2004; Liebethal et al., 2005). However, other studies have identified additional energy sources that can potentially impact the estimated ground heat flux term (Foken, 2008; Meyers & Hollinger, 2004). These include energy stored in an existing snow pack directly above the plate (Hinzman et al., 1998; N. B. Miller et al., 2017; Persson et al., 2002; Westermann et al., 2009), whereby the density and other parameters of the snow pack, such as moisture advection (Helgason & Pomeroy, 2012), could impact flux values. Vegetation is another term that has the potential to influence the storage change term (Heusinkveld et al., 2004; Jacobsen, 1999; Masseroni, Corbari, & Mancini, 2014). Details of the vegetative storage term proposed in different studies range from capturing energy due to photosynthesis to biomass canopies covering the ground heat flux measurement area indirectly impacting the fluxes (Masseroni et al., 2014). Even in Arctic tundra locations, vegetation harnesses, stores, and emits energy that should be accounted for in the surface energy budget, if not directly reflected in the ground heat flux (Jacobsen, 1999; Mikola et al., 2018; Sari et al., 2017). In general, it is clear that other storage change terms might influence the ground heat flux in addition to the energy stored in the soil (S) above the instrument (Foken, 2008), and efforts are ongoing within the flux community to assess their importance. Two publications (Masseroni et al., 2014; Meyers & Hollinger, 2004) go so far as to suggest the inclusion of all of the above mentioned energy storage terms (photosynthesis, biomass canopy, and soil water content) in analyses of the surface energy budget, but not necessarily the ground heat flux term itself even though they might influence the term.

Recall that two methods can be used to measure ground heat flux (Liebethal et al., 2005): flux plates and thermistor temperature probes. Debate continues as to which approach works best (Halliwell & Rouse, 1987; Liebethal et al., 2005; Philip, 1961). As noted, the flux plate method captures the ground heat flux by measuring the temperature gradient across a known material (usually metal or a known composite), and applying a calibration coefficient of the known conductivity of the instruments to obtain the final measurement value (Hukseflux, 2015). By comparison, the thermistor probes capture the ground heat flux by measuring the temperature gradient across a soil layer (of which the soil heat capacity and thermal conductivity should be known for the depth of which the ground heat flux is being measured). One then derives a storage change term to capture the amount of energy stored in the layer of soil above the flux plate using known soil properties and a temperature gradient of the soil to assess storage change (MRC, 2015).

The flux plate method is a continually evolving technology, while thermistor temperature probes have traditionally been used (and are still used) to verify flux plate outputs (Liebethal et al., 2005; Persson et al., 2002; Philip, 1961). Discrepancies arise using the thermistor probe method due to the need for soil property information, thereby requiring soil samples (Evett et al., 2012; Liebethal et al., 2005). Flux plates have been criticized in that their accuracy depends on the material thickness and type of material used (Philip, 1961). Flux plates have also been critiqued for their inability to properly account for difference in soil heat capacity between the soil and the plate itself to account for the energy stored in the soil (S) above the plate (Liebethal et al., 2005). Thus far, the community has failed to adopt a consistent method for measuring ground heat flux. Thermistor temperature probes have been used among the scientific community far longer, and therefore provide a longer data base of ground heat flux data (Carson, 1963; Persson et al., 2002).

A necessary part of understanding the ground heat flux term is sign convention – defining which direction a positive or negative ground heat flux value represents – along with determining the depth and interface level at which the ground heat flux is defined. Most publications adopt the convention (as used here) that a positive ground heat flux is away from the surface, while a negative ground heat flux is toward the surface (see Figure 1) (N. B. Miller et al., 2017; Persson et al., 2002; Peters-Lidard et al., 1998). Similarly, the ground heat flux is defined as a conductive energy exchange at the surface, however, there is an issue of defining what the "surface" is. Researchers typically define the surface as the interface of the atmosphere and soil, excluding additional factors such as vegetation or overlying snowpack (Carson, 1963; Koren, 2007; Nicolsky et al., 2009). The modeling and satellite communities define the ground heat flux as at the interface of the atmosphere and the top of a snow pack (Helgason & Pomeroy, 2012; Muskett, 2015) or the atmosphere and the top of a moss or other vegetation (Mikola et al., 2018; Sari et al., 2017).

Most researchers have concluded that vegetation and the snow pack influence the ground heat flux measurement, but how the ground heat flux level is defined will determine whether or not those terms are included (Heusinkveld et al., 2004; Hinzman et al., 1998; Masseroni et al., 2014). For the present study, the ground heat flux (Q_G) is defined as the energy exchange between the soil and atmosphere at zero cm depth (and will not include vegetative or snow pack storage terms) adjusting for the change in soil storage (S) above the flux plate measurement (G), and a positive flux represents energy directed away from the surface. If vegetation or snow pack exist at the defined ground heat flux level, their storage values will not be included in the adjusted ground heat flux calculation (Figure 1).

Table 1 summarizes the range of ground heat flux values collected from different areas around the globe.

Table 1. Recorded ground heat flux values from previous publications. Note that all fluxes represented in the table do not include a storage change term.

Publication Citation	Range of GHF in W/m^2	Location of Study	Region	Measurement Method	Time Period of Collected Data
Grachev et al., 2017	*-20 to +60*	*Eureka, Canada*	*High-Latitude/Arctic*	Flux Plate	2011
Grachev et al., 2017	*-30 to +60*	*Tiksi, Russia*	*High-Latitude/Arctic*	Flux Plate	2012
Persson et al., 2002	*0 to +20*	*SHEBA/Arctic Ice Sheet*	*High-Latitude/Arctic*	Thermistor	Nov-1997 to Sep-1998
Foken, 2008	-30 to +25	Fresno, California	Mid-Latitude	Thermistor	summer 2000
Miller et al., 2017	*-10 to +10*	*Summit, Greenland*	*High-Latitude/Arctic*	Thermistor	Jul-2013 to Jun-2014
Kustas, Prueger, Hatfield, Ramalingam, & Hipps, 2000	-100 to + 200	Jornada Experimental Range, New Mexico	Mid-Latitude	Flux Plate	
Heusinkveld et al., 2004	-80 to +150	Nizzana, Israel	Mid-Latitude	Flux Plate	Oct-2000
Rouse et al., 2003	*0 to +25*	*Mackenzie River Basin, Canada*	*High-Latitude/Arctic*	Thermistor/Transducer	1997-1999
Helgason & Pomeroy, 2012	*0 to +20*	*Saskatoon, Canada*	*High-Latitude*	Flux Plate	winter 2006/2007
Hinzman et al., 1991	*-10 to +20*	*North Slope Alaska*	*High-Latitude/Arctic*	Thermistors	1985-1989
Boike et al., 2003	*-40 to +40*	*Ny-Alesund, Spitsbergen*	*High-Latitude/Arctic*	Thermistors	Jul-1998 to Jan-2000
Masseroni et al., 2014	-25 to +50	Livraga, Italy	Mid-Latitude	Flux Plate	2012

Some of these include a storage change term (in the soil, vegetation, snow pack or material) while others do not. In a study at Fresno, California, Foken (2008), using a thermistor temperature probe, found ground heat flux (Q_G) values to vary between 20-50 Wm^{-2} with the inclusion of a soil storage change term. Ground heat fluxes (G) measured during the year 2011 from flux plates at Eureka Station in the Canadian Arctic (without a storage term) ranged from -20 Wm^{-2} to +60 Wm^{-2} depending on season (Grachev et al., 2017). The same study found ground heat fluxes (G) collected from flux plates, not including a storage change term, to vary from -30 Wm^{-2} to +60 Wm^{-2} in the year 2012 at the Tiksi observatory (the same station being evaluated in the present study) (Grachev et al., 2017). During the SHEBA campaign in the Beaufort Sea, surface heat fluxes through the sea ice cover using a thermistor temperature probe and no storage change term, ranged from 0-20 Wm^{-2} (Persson et al., 2002).

3. Research Design

3.1 Objective: Research Questions

Data have been collected at Tiksi since 2011, but this study focuses on the year 2016 since it provides the most complete annual record. In the years preceding 2016 there were power or instrument outages as well as heaving of instruments to different levels within the soil. Using soil flux plate instruments, this thesis addresses the following research objectives and hypotheses:

Objective 1. Analyze the spatial variability of the ground heat flux at the Tiksi observatory in summer, winter, and during the transition seasons.

Expectation 1-1: Ground heat flux soil variables (soil thermal conductivity and heat capacity) change with respect to soil moisture content and soil organic/mineral type, which previous work indicates are highly variable in the vicinity of the Tiksi observatory (Mikola et al., 2018; Sari et al., 2017).

Therefore, ground heat flux values are expected to also vary with respect to location around Tiksi.

Expectation 1-2: A more representative regional ground heat flux for the Tiksi observatory can be calculated as the area-weighted average of the fluxes measured in the land cover types found in the vicinity.

Objective 2. Analyze the temporal variability for a full annual cycle of ground heat fluxes for each land cover type at the Tiksi observatory.

Expectation 2-1: The ground heat flux will attain small or negative 30-minute values during the winter months since water content in the soil will freeze as energy is lost from the soil (Halliwell & Rouse, 1987; Putkonen, 1998). This result is expected in all saturated land cover types.

Expectation 2-2: The spatial variability in the ground heat flux between land cover types is large relative to the temporal variability of any one land cover type, and the magnitude of the ground heat flux will be proportional to soil moisture.

Expectation 2-3: The spring transition in the ground heat flux is expected to be abrupt from negative to positive values in accordance with the rapid transition from a snow-covered to snow-free surface whereas the autumn transition will be dominated by the zero-curtain effect. Thus is due to turbulent fluxes decreasing rapidly from summer values (Grachev et al., 2017), the duration of which is expected to be related to soil moisture content.

Objective 3. Conduct an uncertainty analysis of the ground heat flux measurement.

Expectation 3-1: It is anticipated that the ground heat flux in the vicinity of Tiksi is large enough to be measurable with available instruments.

Expectation 3-2: Flux plates will provide more accurate results than the common method based on thermistor probes because the flux plate provides a direct measurement with fewer required assumptions.

3.2 Tiksi Station Overview

The Russian Tiksi observatory (Figure 2) is located at 71.6N, 128.9E (IASOA, 2015).

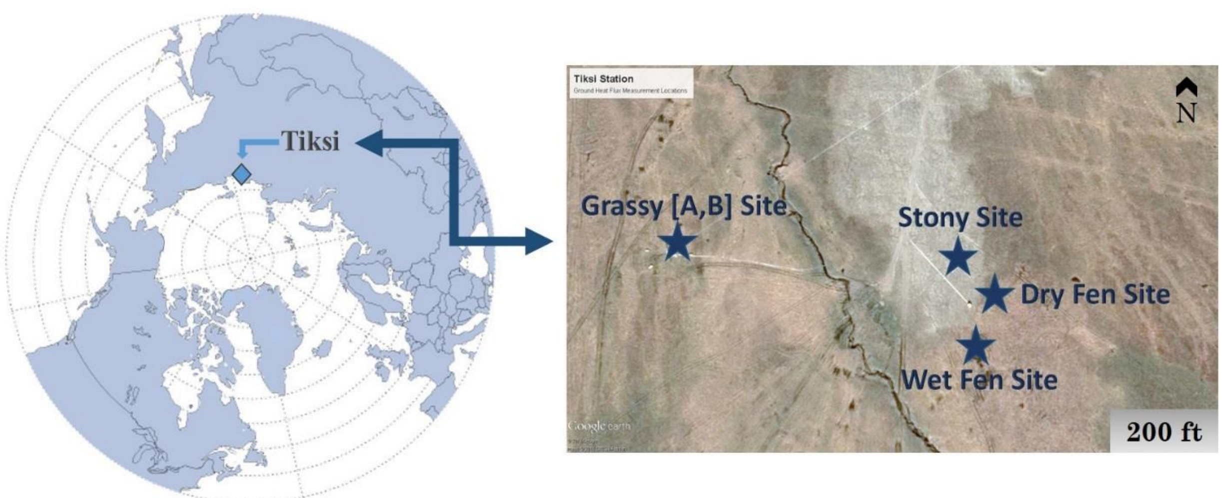

Figure 2. The Russian observatory, Tiksi is a high-latitude observatory located in the Siberian Arctic. There are four sub-stations where ground heat flux is measured using flux plate instruments. The Grassy site has two flux plates that are identified as GrassyA and GrassyB.

The observatory supports a wide suite of additional instruments, but the most important instruments for this project are installed at the base of a 20-meter-tall meteorological flux tower with three other soil flux suites located near the tower (see Figure 2). Ground heat flux measurements are made at four sites, using one Hukseflux HFP01 flux plate installed at 5 cm depth at each location (with one location utilizing two flux plates for instrument comparison), and an additional skin and soil temperature probe at each location. The sites are spread across an approximate area of 2 kilometers x 2 kilometers. The landscape around the Tiksi flux sites range in elevation from near zero to twelve meters above sea level. The topography is generally uniform with rolling hills surrounding the observatory and vegetation in the form of short tundra grasses and shrubs in summer, while during the winter the ground is primarily snow and ice covered (Figure 3a and 3b).

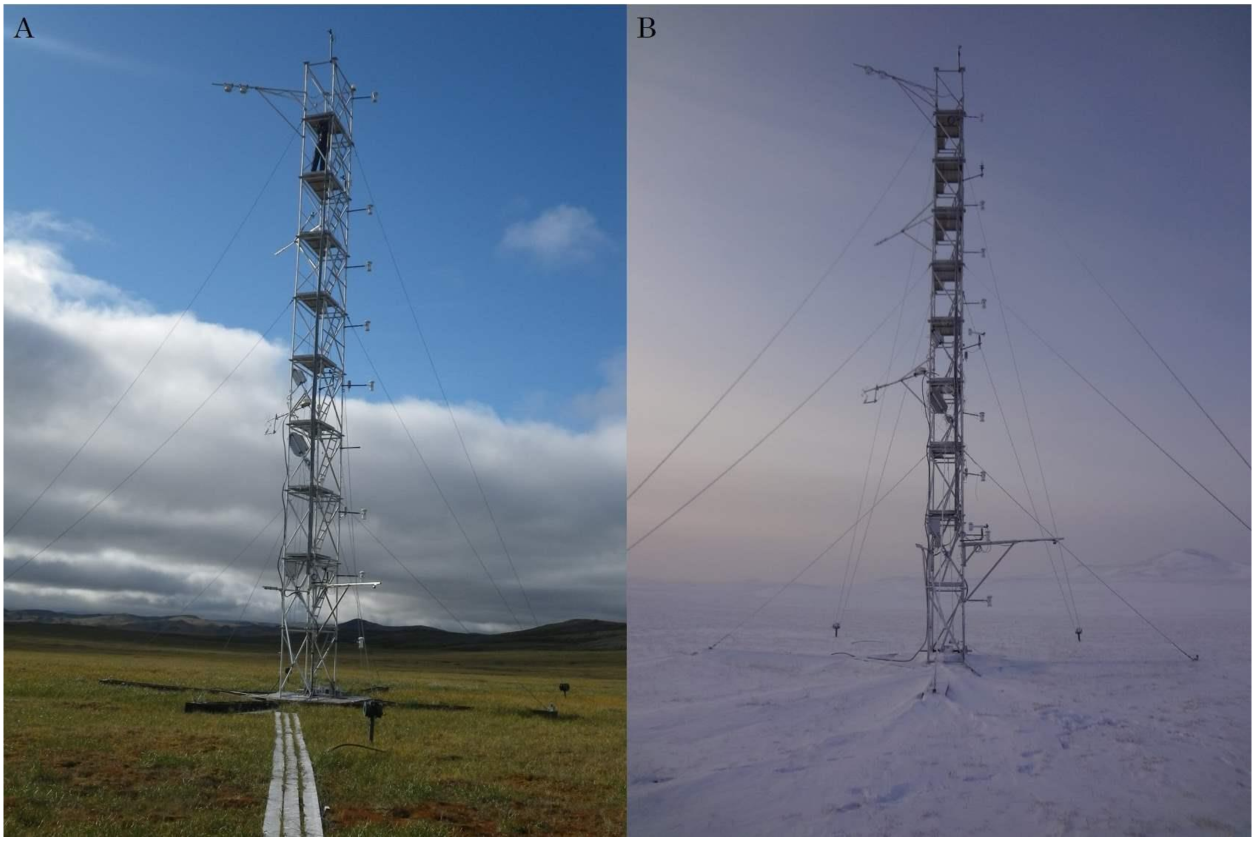

Figure 3. These photographs were taken of the flux tower facility at the Tiksi observatory in 2013/2014. The photograph on the left (**A**) was taken in August and the photograph on the right (**B**) was taken in March, both with the same orientation to the tower. The GrassyA and GrassyB flux plates were installed in the soil at the base of the flux tower in 2011.

Tiksi observatory is hosted by the Federal Service for Hydrometeorology and Environmental Monitoring (Roshydromet) in Russia, who collaborate directly with both the National Oceanic and Atmospheric Administration (NOAA) in the United States and the Finnish Meteorological Institute (FMI) in Finland. NOAA worked closely with Roshydromet to facilitate building the 20 meter meteorological tower in 2010, where the NOAA-based flux measurements are housed. FMI worked in parallel with Roshydromet to complete the other three flux sub-stations in 2012 where the FMI-based flux measurements are located. In 2014, a map of the surrounding area of Tiksi was generated using both field data and satellite remote sensing via World View-2 (Mikola et al., 2018; Sari et al., 2017) (refer to Section 3.4 below for more details).

Tiksi observatory was chosen for this study due to the unique collaboration between NOAA, Roshydromet, and the FMI, in which data are collected in near-real time from flux platforms and where land classification analyses are already in progress (Mikola et al., 2018). Two of the flux plate instruments were installed at 5 cm depth next to each other at the base of the flux tower in 2010 for instrument comparisons. The other three flux plates were installed in 2012 at 5 cm depth and were repositioned in 2015 back to a depth of 5 cm after frost heaving in the area uprooted the instruments (IASOA, 2015; Laurila, 2015). Data from the observatory is wirelessly transferred back to the NOAA-Physical Sciences Division every six hours and is plotted at NOAA on a daily basis. Due to the difficult environment, maintaining power can be challenging. During 2016 there were power outages due to weather and site maintenance, and data could not be collected or recovered for the following periods: Day of Year (DOY) 1-12, DOY 183-194, DOY 226-228, and DOY 310-319. These data gaps account for a loss of 34 days or ~10% of data for the year 2016. Tiksi experiences power outages quite regularly due to its location, which means that finding an uninterrupted annual cycle of data at the observatory is almost impossible. Additionally, due to the relatively new infrastructure, several instrument suites experienced problems with structures and instruments settling into the active layer. This settling and heaving of the soil uprooted many of the flux plates to unknown depths, therefore analyzing and reconstructing those data sets would not have provided meaningful results (Aurela, 2017b; Laurila, 2015), and it was for this reason that the year 2016 was chosen (it was the most consistent year for both data collection and instrument stability). Of the NOAA Arctic station managed by the Physical Sciences Division, Tiksi observatory is outfitted with the most flux plates, five in total.

As noted, Tiksi observatory has several facilities on-site and a vast range of meteorological instruments. The flux tower is outfitted primarily with wind sensors, temperature and humidity sensors, sonic anemometers, a CO_2 sensor, and a thermistor temperature probe (IASOA, 2015). Additionally, Tiksi is a registered Baseline Surface Radiation Network (BSRN) station with shortwave, longwave, diffuse, and direct solar radiation measurements (IASOA, 2015). Tiksi also hosts a Climate Reference Network (CRN) complete with precipitation, wind, and solar radiation instruments (IASOA, 2015). The observatory also collects aerosol, ozone, and air samples that are analyzed at by NOAA and FMI researchers (IASOA, 2015).

3.3 Observation & Instrument Details

As shown in Figure 4, the ground heat flux instruments are located in four of the nine identified land cover types (two flux plates are positioned in the Grassy land cover type): Stony, Grassy, Dry Fen, and Wet Fen.

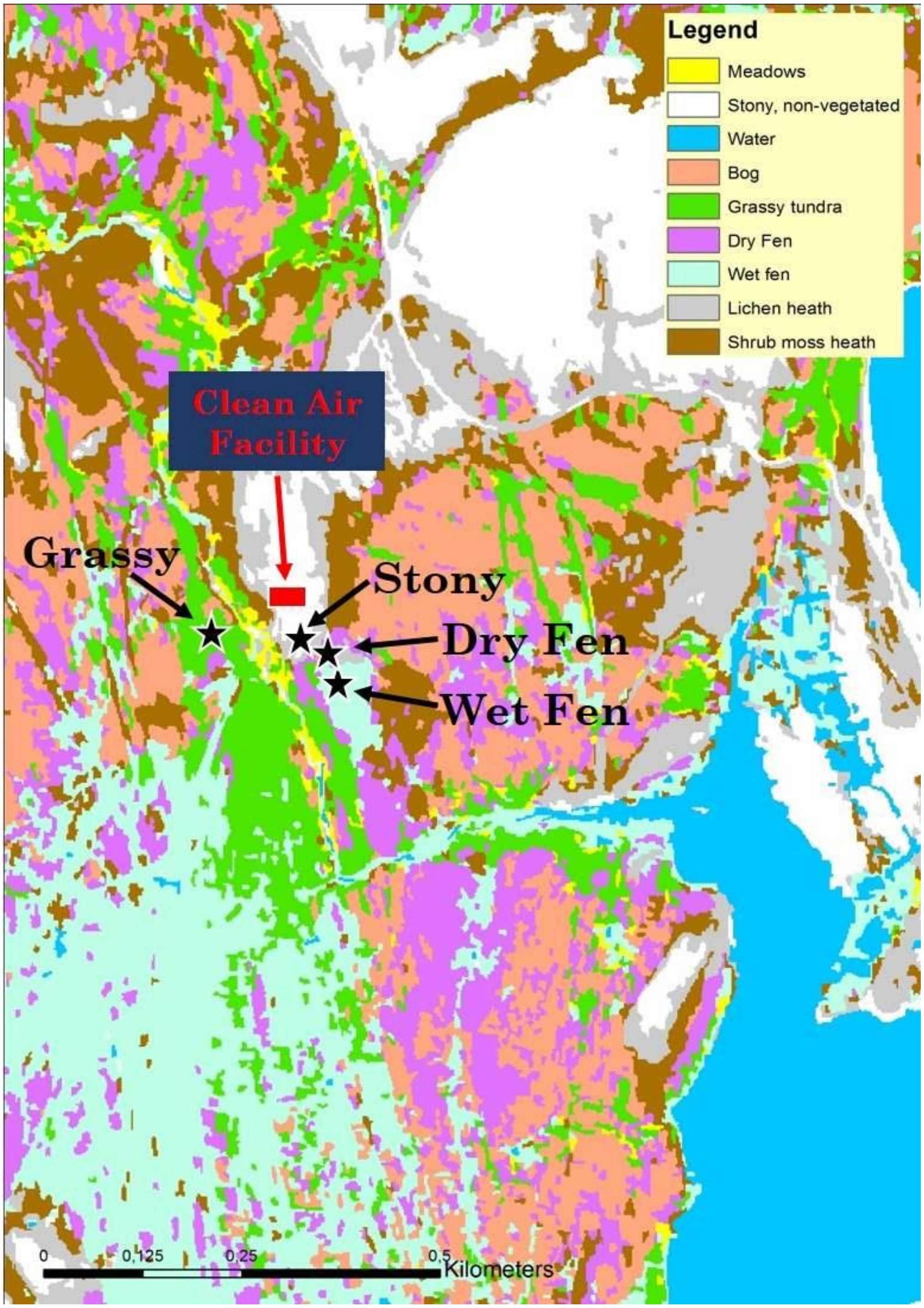

Figure 4. Map output from Mikola et al. (2018) study showing the nine land cover types in the vicinity of the Tiksi observatory. Labeled within the identified area are the four sub-stations where ground heat flux is measured; names of the sub-stations are directly related to the land cover type where they stand. In relation to these sub-stations is also one of Tiksi's primary meteorology buildings, the Clean Air Facility. Ground heat flux is measured in four land cover types: Stony, Grassy, Dry Fen and Wet Fen.

Figure 4 was analyzed by Mikola et al. (2018) to assess the sub-area of each land classification by assigning an image value to each identified color type and then counting those pixels to determine the area percentage of each land classification (Aurela, 2017b). After analyzing the quantity of pixels of each of the land cover types from Figure 4 it was determined that the four instrumented land cover types represent 49% of the 2.79 km^2 study area (see Table 2) leaving 51% unrepresented by ground heat flux measurements.

Table 2. Area break-down of the map in Figure 4 provided by Aurela (2017b) and Mikola et al. (2018). In bold-italic are those land cover types where ground heat flux is measured. Image values were selected to correspond to map color, and the count of the subarea (land cover type) was deduced from the identified color pixel image values within the map area. Area percentage was then derived by converting the count subarea.

Total Area: 2.79 km^2			
Land Cover Type	**Image Value**	**Count, subarea**	**% of area**
Meadows	3	6669	0.96
Stony	***4***	***77879***	***11.16***
Water	5	85093	12.2
Bog	12	99937	14.32
Grassy Tundra	***22***	***55976***	***8.02***
Dry Fen	***111***	***77054***	***11.04***
Wet Fen	***112***	***128022***	***18.35***
Lichen Heath	211	54252	7.78
Shrub Moss Heath	212	112798	16.17
			Total = 100%

The flux plates being analyzed collect data every 1-minute, and are averaged to 30-minute averages in post-processing. Likewise, the soil and skin temperature instruments also collect data every minute, with 30-minute averages calculated in post-processing. All flux plates were installed at a depth of 5 cm, and the Nokeval temperature probes used to capture the skin temperature at the Stony, Dry Fen, and Wet Fen sites were installed directly on top of the soil, while the Apogee skin temperature sensor was installed 2 meters above the soil looking downward. A complete outline of instrument details are provided in Table 3.

Table 3. List of instruments at Tiksi that measure ground heat flux and the corresponding storage term. All instrument were factory calibrated prior to being installed. Calibration coefficients from the resulting factory calibrations are applied in post-processing.

Land Cover Type at Tiksi Station	Instrument Manufacturer	Instrument Type	Parameters	Instrument Description	Depth of Instrument [m]	Sampling Rate	Averaging Period
Stony	Hukseflux	*HFP01*	G	Flux Plate	0.05	1 min	30 min avg
	Nokeval	*PT100*	T_n	Temperature Probe	0.05, 0.10	1 min	30 min avg
	Nokeval	*IKES PT100*	T_{Sfc}	Skin Temperature Probe	Sfc	1 min	30 min avg
Grassy	Hukseflux	*HFP01*	G	Flux PlateA	0.05	1 min	30 min avg
	Hukseflux	*HFP01*	G	Flux PlateB	0.05	1 min	30 min avg
	MRC	*TP101*	T_n	Thermistor Probe	0.05, 0.10, 0.15, 0.20, 0.25, 0.30, 0.45, 0.70, 0.95, 1.2	1 min	30 min avg
	Apogee	*IRTS-P*	T_{Sfc}	Infrared Skin Temperature Sensor	+ 3.3 height	1 min	30 min avg
Dry Fen	Hukseflux	*HFP01*	G	Flux Plate	0.05	1 min	30 min avg
	Nokeval	*PT100*	T_n	Temperature Probe	0.05, 0.10, 0.20, 0.30, 0.40	1 min	30 min avg
	Nokeval	*IKES PT100*	T_{Sfc}	Skin Temperature Probe	Sfc	1 min	30 min avg
Wet Fen	Hukseflux	*HFP01*	G	Flux Plate	0.05	1 min	30 min avg
	Nokeval	*PT100*	T_n	Temperature Probe	0.10, 0.20, 0.40	1 min	30 min avg
	Nokeval	*IKES PT100*	T_{Sfc}	Skin Temperature Probe	Sfc	1 min	30 min avg

The flux plates (Hukseflux: HFP01) feature a thermopile sensor that measures the temperature difference between the top and bottom of the plate. The instrument output is recorded in millivolts and a calibration factor from the manufacturer is applied to convert the heat flux to units of Wm^{-2}. Note that the soil thermal conductivity is not needed when using a flux plate to measure ground heat flux; the thermal conductivity constant is represented in the calibration coefficient of the flux plate itself (the conductivity coefficient is related to the flux plate's material and not the soil) (Hukseflux, 2015). Additionally, soil thermistor temperature strings (MRC: TP101) have been installed at the observatory near each of the flux plates to measure temperature at specific depths and to also measure the storage change term (MRC, 2015). At Tiksi, only one of the sites has the devices vertically strung together (Grassy) in this fashion, while the other sub-stations instead use separated individual probes (Nokeval: PT100) placed at specific depths. Issues arose over the course of the analysis with these individual thermistor probes (Nokeval: PT100) due to heaving that occurred at different levels in the heterogeneous soil matrix. As such, over the course of an annual cycle it was unclear what specific depth each probe was actually measuring (Laurila, 2015). This problem is mitigated in the MRC thermistor string since the temperature sensor levels are fixed within an epoxy tube. As such, if the thermistor string is heaved, then all levels are equally impacted (Laurila, 2015; MRC, 2015). From these measurements, a Fourier analysis is used to derive the difference between the temperature values at each depth with respect to time (Halliwell & Rouse, 1987; Hinzman et al., 1991; Putkonen, 1998).

Tiksi observatory also provides data on surface skin temperature using two different instruments across the different types of soil: 1) Nokeval skin surface probes, 2) an Apogee infrared temperature sensor. At the Tiksi observatory, three Nokeval surface skin temperature probes (Nokeval IKES PT100) are physically located on the surface, so when snow begins to fall in autumn the sensors get buried and no longer directly measure skin temperature (Nokeval, 2015). It was not investigated how solar heating in summer might have adversely impacted these measurements. Additionally, the Tiksi observatory has one Apogee surface skin temperature infrared sensor (Apogee IRTS-P) mounted at two-meter height on the tower structure looking directly down at the surface above the flux plates. However, during winter when there is snow, the sensor does not see the ground surface but rather the snow surface (Apogee, 2015). Thankfully, Tiksi has the infrastructure to compare results from the two methods of collecting skin temperature (see Section 5.2). The skin temperature data for both methods (Nokeval and Apogee) were collected every 1-minute (with 30-minute averages calculated in post-processing).

3.4 Tiksi Land Classification

Techniques for land classification for this study originated from FMI through their collaborative effort with Mikola et al. (2018). This section summarizes the results from the study completed by Mikola et al. (2018) (shared by Mika Aurela – FMI affiliation) who used both field measurements and satellite techniques to estimate land cover types in the area surrounding the Tiksi observatory. The on-site field measurements were collected in the summer of 2014 by surveying the designated area and classifying the different land cover types. These classifications were defined by soil density, organic matter concentration and leaf litter area (among other biological categorization processes) which are detailed later below.

The maps provided by Mikola et al. (2018) are used here to identify the land cover types that each ground heat flux measurement represents to identify how different land covers might impact soil ground heat flux. Since ground heat flux measurements are not available in all of the land cover types, one can only capture the area-weighted average from the land cover types in which fluxes were measured. The map from Mikola et al. (2018) provided soil categories for a 2.79 km^2 area, and by spatially extrapolating the ground heat flux measurements to the area of the land cover class it is assumed that the plates account for 49% of the maps area (Aurela, 2017b; Mikola et al., 2018). The map will be utilized as the primary source of imaging and soil categorization for the remainder of the study.

A total of 92 plots were investigated through a field survey around the area where the flux measurements were taken. The majority of the plots were defined via a measurement design where samples were analyzed at set distances along transects. Once the plots were selected, a visual inspection was used to assess the plant and soil characteristics. The following tundra land cover types were chosen for the area: Meadows, Stony (non-vegetated), Water, Bog, Grassy Tundra, Dry Fen, Wet Fen, Lichen Heath, and Shrub Moss Heath.

Three remote sensing tools were used to create the land classification maps: QuickBird, WorldView-2 and a digital elevation model (DEM). QuickBird and WorldView-2 provided high resolution satellite images; WorldView-2 images were recorded with a resolution of 2-meters and QuickBird images were recorded with a resolution of 0.6-meters. Images were obtained for different years to assess the landscape's evolution, including changes in seasonal growth. The QuickBird images were collected in the early growing season of spring 2005 to capture the early stage of growth, while the WorldView-2 images were collected at two later time periods, summer of 2012 and 2015, to capture later stages of growth. The DEM, with 2-meter resolution, was used to capture influences from the surrounding topography on the soil during the summer of 2015. The DEM was used to model topography, solar radiation, elevation, and slope; the visualization techniques utilized processing procedures from Erdas Imagine, ArcGIS 10.3.1 and SAGA-GIS 2.1.2 (Mikola et al., 2018). Together, the QuickBird, WorldView-2, and the DEM data were analyzed in parallel with the field data that was also collected to produce the vegetation map shown in Figure 5.

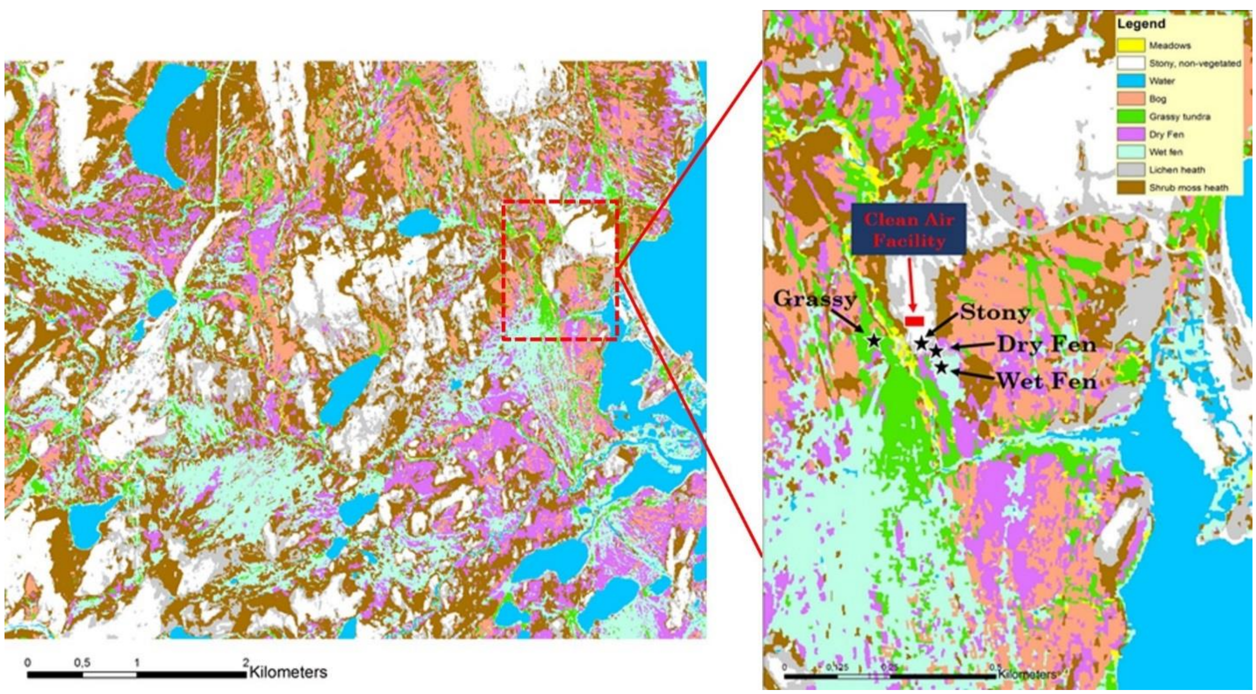

Figure 5. A map of the land classifications provided by Mikola et al. (2018). The entire land classification map completed in 2014-2015 is seen on the left, while the map on the right shows the area of the Tiksi observatory. These maps utilized a combination of satellite techniques and on-site field measurements.

Based on the land cover categories defined by Mikola et al. (2018), the leaf area index (LAI) of the shrubs and mosses in the area was smallest in the stony and lichen heath land cover types and highest in the meadow and wet fen classifications. LAI and vascular shoot mass values were determined by collecting the biomass from field plots and then scanning the biomass to identify pigments within the images (Sari et al., 2017). The species composition within the land cover types did not differ from one soil category to the next, meaning that the same plant type was found among several land covers. The thaw depth of the active layer was measured in the summer of 2014 using an iron rod probe and temperature measurements. It was concluded that the meadow and wet fen categories had a deep thaw layer, while the stony and tundra categories had a shallow thaw layer; thaw layer was influenced by soil temperature, such that drier soils had higher soil temperatures and wetter soils had lower soil temperatures. A primary conclusion drawn from the mapping study was that there is large spatial variation in vegetation surrounding the Tiksi observatory. This mapping exercise highlighted the necessity of comparing field-data to remote sensing data, i.e. field-data can only capture a small area, and satellite remote sensing covers a larger area, but can be influenced by cloud cover thereby limiting when useful images can be collected. Results from the soil characteristic analysis completed during the Mikola et al. (2018) study follow in Table 4 (Aurela, 2017a).

Table 4. Soil classification details provided by Aurela (2017b). Classifications are primarily denoted by vegetation type and quantity. Sub-sites where ground heat flux is measured are in bold-italics.

Land Class	Class Definitions	Class Type	Class Description	Vascular Shoot Mass and Characterization	Soil Organic Matter (SOM) Concentration %	Thaw Depth Averages
Peatlands	Noticeable peat layer; peat forming plants and shrubs	***Dry Fen***	Water surface below the moss layer, some shrubs may occur	53 g m^{-2} Intermediate	38%	35 cm
		Wet Fen	Water surface high, often water pools; some mosses	91 g m^{-2} High	38%	42 cm
		Bog	Drier peatlands, hummock-hollow patterns; dwarf shrubs common	91 g m^{-2} Intermediate	38%	35 cm
Moorlands/Heaths	Dry areas, thin humus layer, no peat formation, mineral soil close to soil surface; shrubs dominate along with annuals, grasses, heath mosses, lichens	Lichen Heath	Lichen dominated, but also few dwarf shrubs, annuals and mosses; often in patches within bare ground	53 g m^{-2} Low	3.90%	26 cm
		Shrub-Moss Heath	Shrub dominated, but also lichens, annuals and mosses	91 g m^{-2} Intermediate	21%	26 cm
		Grassy Tundra	Grass dominated areas; shrubs, annuals and other vascular plants may occur	91 g m^{-2} Intermediate	38%	35 cm
Meadows	Riverside spring flooding areas, drier during growing season	Flood Meadow	Grass dominated, annuals occur, brown mosses	91 g m^{-2} High	21%	42 cm
Bare Soil	Non-vegetated	***Stony***	Non-vegetated	7 g m^{-2} Low	3.90%	26 cm
Water	Water	Water	Water	n/a	n/a	n/a

4. Methods

4.1 Skin Temperature Accuracy

Since skin temperature is important for deriving the storage change term, it is important to assess the accuracy of the instrument measuring this variable. Validation of the infrared skin temperature data from the Apogee sensor proved difficult since it is the only instrument of its kind on site. However, by using data collected from an upwelling (downward facing) longwave BSRN radiometer on-site it was possible to derive skin temperature at the surface for instrument verification. The flux from the radiometer was used to quantify the surface temperature recorded from the instrument. This method was only possible for comparison with the infrared skin temperature sensor (Apogee) and not the skin temperature based on the probes (Nokeval). This is because the upwelling longwave radiometer temperature measurement captures the skin temperature of the surface in a method similar to the infrared sensor; the infrared skin temperature sensor and the upwelling longwave radiometer sensors both seek to capture the surface temperature, whether or not that surface is soil, snow, or vegetation.

The infrared sensor (Apogee) collects data at a spectral frequency of 8 – 14 micrometers with a half-angle field of view of 22°, while the upwelling longwave radiometer sensor collects data at a frequency of 4 – 50 micrometers with a 180° field of view. The other method of capturing skin temperature, using a probe positioned directly at the surface (Nokeval), could not be compared to the infrared temperature sensor since the instruments did not measure skin temperature at the same interface. By taking the recorded energy flux from the BSRN radiometer and using the Stefan-Boltzmann equation one could arrive at:

$$T_{skin} = (UWLW/\sigma^*\varepsilon)^{0.25} \tag{6}$$

Where **UWLW** is the upwelling longwave energy flux in Wm^{-2}, $\boldsymbol{\sigma} = 5.6704*10^{-8}$ is the Stephan-Boltzmann constant and the emissivity $\boldsymbol{\varepsilon}$ is taken at 0.985 assuming that the ground is snow-covered (Dozier & Warren, 1982). Results of this comparison are summarized in Figure 6.

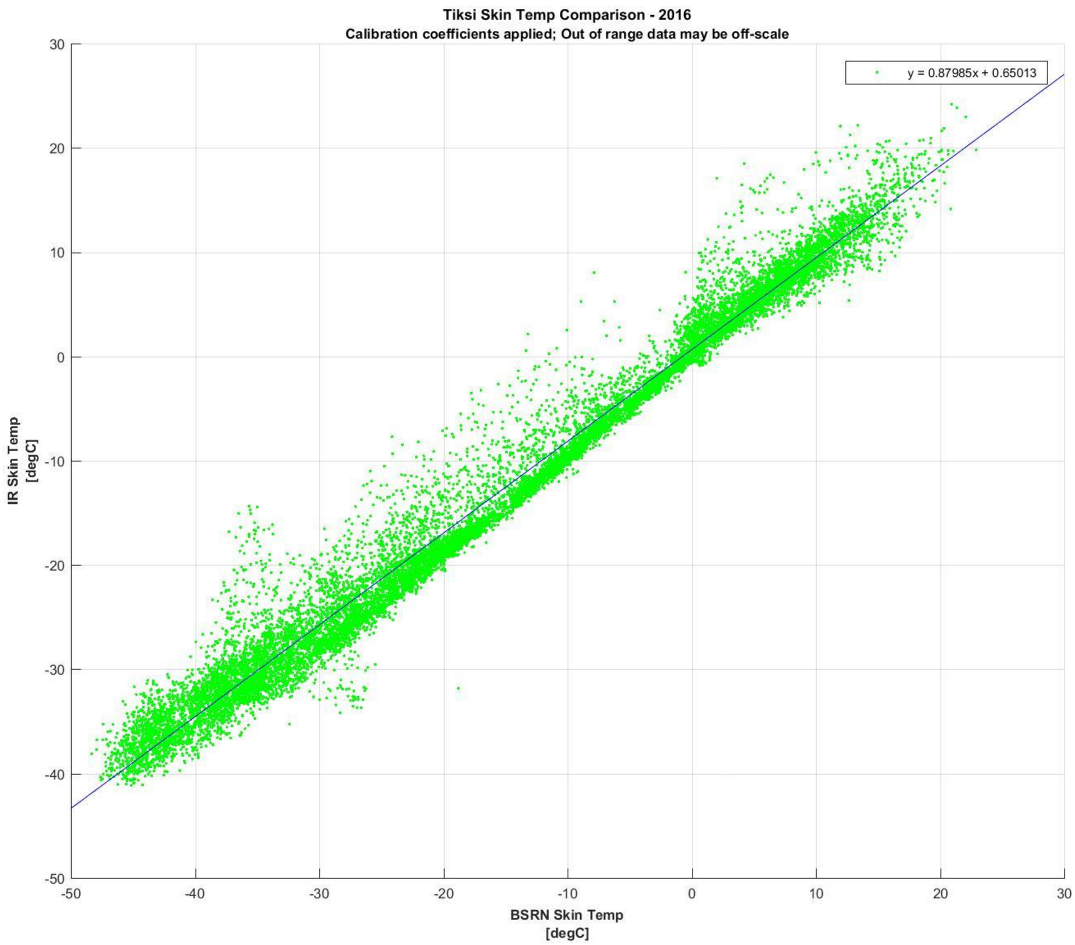

Figure 6. Direct comparison of the infrared (Apogee) skin temperature to the skin temperature derived from the upwelling longwave radiometer on-site.

Visually, there is a good match between results from the infrared skin temperature sensor and temperature based on the upwelling longwave radiation. From the figure it is apparent that the Apogee sensor tends to measure higher temperatures at lower temperatures when compared to the derived skin temperature.

Similarly, data from the Apogee infrared skin temperature sensor were compared to the other Nokeval skin temperature probe used at the Stony, Dry Fen, and Wet Fen sites. These results showed a non-linear relationship (Figure 7) due to the nature of how the two different sensors observe and define the skin surface.

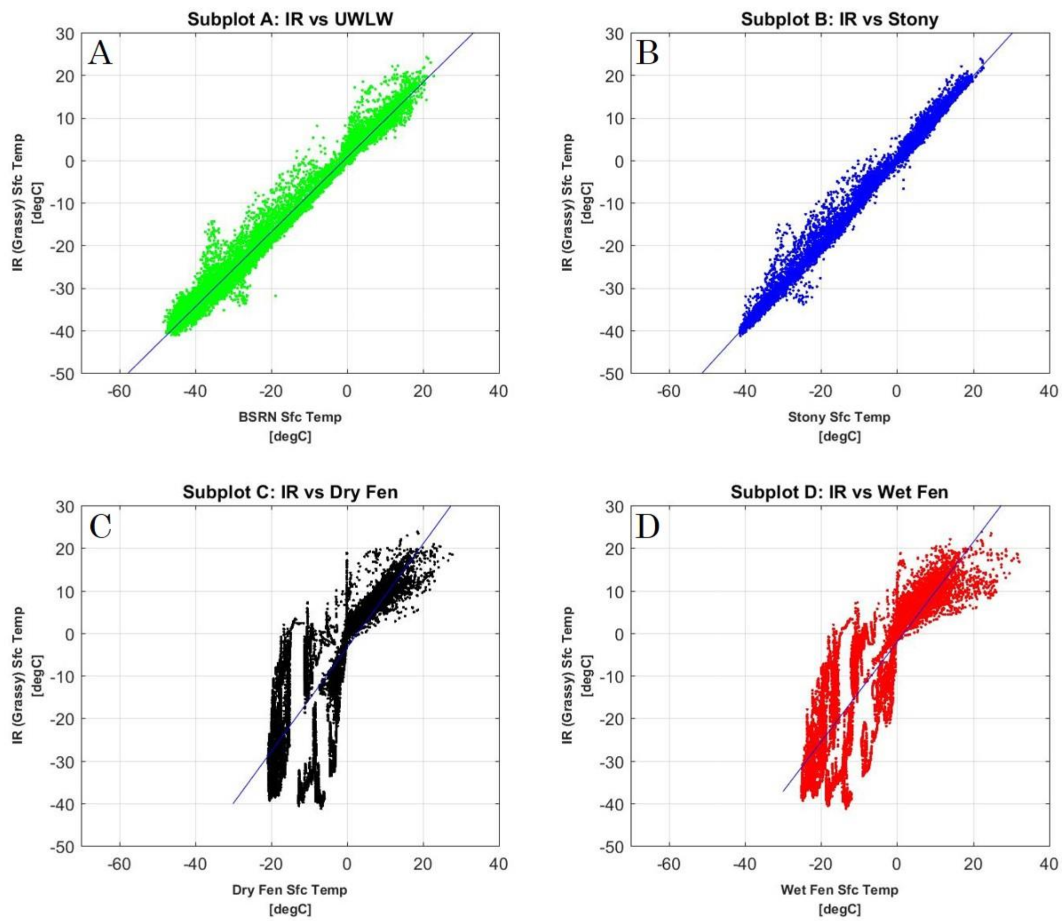

Figure 7. Direct comparison of the infrared (Apogee) skin temperature to the upwelling longwave derived skin temperature from BSRN (**A**). Direct comparison of the infrared (Apogee, y-axis) skin temperature to the skin temperature probe (Nokeval, x-axis) (**B-D**). Sub-plots (**B-D**) represent each of the identified land cover types utilizing the Nokeval skin temperature sensor.

Meaning that because the Apogee sensor, located 2-meters above the ground, measures skin temperature from above looking down, it will measure the temperature of whatever is directly below the sensor (i.e. snow pack, vegetation, soil, etc.). By comparison, the Nokeval sensor measures skin temperature directly (this sensor is placed directly on top of the soil, so in winter it can become buried by the snow).

When the infrared temperature sensor was compared to the Nokeval temperature probe, it compared well for the Stony land cover type (Figure 7B), but not well with the other two saturated land cover types. The discrepancies in the two saturated land cover types (Figure 7C and 7D) were primarily limited to winter, when the infrared skin temperature sensor (Apogee) was measuring a skin temperature from above looking down at the assumedly snow-covered surface, and the Nokeval sensor was measuring a skin temperature from beneath the snow. The results in Figure 7C and 7D show how the snow provides an insulating layer above the ground surface and degrades the correlation between the two methods of measuring skin temperature. It hence seems appropriate to continue to use both the Apogee and Nokeval skin temperature sensors to represent skin temperature at each of the land cover sites since each was positioned in tandem with a corresponding flux plate at each site (it was important that skin temperature was measured at the exact location of each flux plate regardless of method).

Table 5 provides a detailed comparison of temperatures from the different methods, including r^2 values to determine how closely related the two methods are, and also the root-mean-square (RMS) difference to assess differences between the values and therefore the differences between the instruments.

Table 5. Output comparisons of each type of skin temperature sensor to evaluate how the different instruments compare to one another.

Measurement Type	Comparison	r^2	RMS Difference [degC]
Skin Temp	T_{IR} / T_{BSRN}	0.98	4.06
	T_{stony} / $T_{dry\ fen}$	0.68	10.9
	T_{stony} / $T_{wet\ fen}$	0.76	9.17
	$T_{dry\ fen}$ / $T_{wet\ fen}$	0.95	3.01

It is seen that the Apogee skin temperatures compare relatively well to the upwelling longwave-derived temperatures, with an r-squared value of 0.98. Additionally, the RMS analysis showed a difference of 4.06°C between the two methods (Apogee vs BSRN) over the course of the annual cycle. The other comparisons were done for the Nokeval sensors located at the other land cover types. It was interesting to compare values from the same sensor type to see the impact from different land cover types. The results showed that the two saturated sites (Dry Fen and Wet Fen) correlated well to one another given their high r-squared value and low RMS temperature difference.

4.2 Soil Property Assessment

The storage change term is derived for flux plates by measuring the difference in the temperature gradient over time within the layer of soil depth directly above the flux plate and then applying a soil heat capacity value for that specific type of soil (Blanken, 2015; Liebethal et al., 2005) (see Equation 4 in Section 1.1). By comparison, when using thermistor strings one needs to know both the soil heat capacity and the thermal conductivity of the soil since the temperature gradient being measured is not across a material with known thermal characteristics, but a soil (Hinzman et al., 1998; Persson et al., 2002). Regardless of the flux measurement method, this storage change term must be included in the overall ground heat flux (Q_G) measurement to capture energy gained or lost to the system (S) within the shallow layer of soil directly above the soil flux plate/thermistor (G) (Blanken, 2015).

Since the storage change term (S) requires knowing the soil properties to calculate soil storage, it is optimal to directly measure these parameters at the location of the flux plates. However, since Tiksi observatory does not allow for removal of soil samples for testing, results from the literature were used for soils similar to those found at Tiksi (Table 6).

Table 6. Table of collection of measured soil heat capacity and thermal conductivity. Those rows in bold highlight data collected in Arctic regions. The row highlighted in green correspond to the soil parameters used in the study at Tiksi.

		K_sl [Wm-1K-1]			*C_psl [(x 10^6) Jm-3K-1]*			
Publication Defined Land Class (Region)	**Publication Site Description (including depth [m])**	**Thermal Conductivity [generic]**	**Thermal Conductivity [frozen]**	**Thermal Conductivity [thawed]**	**Heat Capacity [generic]**	**Heat Capacity [frozen]**	**Heat Capacity [thawed]**	**Author/Publication**
Tundra (Northslope, Alaska)	mineral/organic	0.7 - 1.8						Cable, 2010
Tundra (Northslope, Alaska)	mineral/silt	1.3 - 2.4						Cable, 2010
Tundra (Northslope, Alaska)	mineral/gravel	2.5 - 3.5						Cable, 2010
Tundra (Northslope, Alaska)	mineral/shale	1.0 - 2.0						Cable, 2010
Location unknown	snow parameter	3.44			2.19			ECMWF, 2004
Tundra (Fairbanks, Alaska)	organic		0.12	0.29				Farouki, 1981
Tundra (Fairbanks, Alaska)	mineral		1.05	0.89				Farouki, 1981
Tundra (Northslope, Alaska)	quartz	8.79						Sellers, 1965
Tundra (Northslope, Alaska)	mineral/clay	2.93						Sellers, 1965
Tundra (Northslope, Alaska)	organic	0.25						Sellers, 1965
Tundra (Northslope, Alaska)	water	0.57						Sellers, 1965
Tundra (Northslope, Alaska)	ice	2.17						Sellers, 1965
Tundra (Northslope, Alaska)	air	0.025						Sellers, 1965
Soil at 20 degC (location unknown)	mineral				1.9			Kluitenberg, 2002
Soil at 20 degC (location unknown)	organic				2.5			Kluitenberg, 2002
Soil at 20 degC (location unknown)	water				4.18			Kluitenberg, 2002
Soil at 20 degC (location unknown)	ice				1.9			Kluitenberg, 2002
Soil at 20 degC (location unknown)	air				0.0012			Kluitenberg, 2002
SHEBA Ice Sheet (Arctic)	snow cover	0.3						Persson et al., 2002
SHEBA Ice Sheet (Arctic)	ice	2						Persson et al., 2002
Estimate from land-surface model	mineral/dry				1.26			Wang & Bou-Zeid, 2012
Estimate from land-surface model	mineral/wet				4.2			Wang & Bou-Zeid, 2012
Tundra (Northslope, Alaska)	**barren**		**0.54**	**0.39**		**9.91**	**4.86**	**Hinzman et al., 1998**
Tundra (Northslope, Alaska)	**moist acidic**		**0.58**	**0.38**		**8.11**	**1.24**	**Hinzman et al., 1998**
Tundra (Northslope, Alaska)	**moist non-acidic dry**		**0.81**	**0.43**		**1.31**	**1.64**	**Hinzman et al., 1998**
Tundra (Northslope, Alaska)	**shrublands**		**0.58**	**0.34**		**8.11**	**1.24**	**Hinzman et al., 1998**

Table 6. Continued

		K_sl [Wm-1K-1]			C_psl [(x 10^6) Jm-3K-1]			
Tundra (Northslope, Alaska)	wet		0.64	0.47		1.25	1.14	Hinzman et al., 1998
Tundra (Northslope, Alaska)	water		3.85	1.24		4.89	3.23	Hinzman et al., 1998
Tundra (Manitoba, Canada)	Churchill site: peat (depth: 0-0.3)		1.6	0.6	2.5			Halliwell & Rouse, 1987
Tundra (Manitoba, Canada)	Churchill site: clay (depth: 0.3-1.0)		2.9	2.3	1.9			Halliwell & Rouse, 1987
Tundra (Manitoba, Canada)	Churchill site: clay (depth: >1.0)		2.9	2.3	1.9			Halliwell & Rouse, 1987
Tundra (Manitoba, Canada)	Marantz site: peat (depth: 0-0.05)		0.4	0.1	2.5			Halliwell & Rouse, 1987
Tundra (Manitoba, Canada)	Marantz site: peat (depth: 0.05-0.08)		0.6	0.3	2.5			Halliwell & Rouse, 1987
Tundra (Manitoba, Canada)	Marantz site: peat (depth: 0.08-0.15)		1.4	0.43	2.5			Halliwell & Rouse, 1987
Tundra (Manitoba, Canada)	Marantz site: peat (depth: >0.15)		1.6	0.56	2.5			Halliwell & Rouse, 1987
Tundra (Svalbard, Norway)	water				4.2			Westermann et al., 2009
Tundra (Svalbard, Norway)	ice				1.9			Westermann et al., 2009
Tundra (Svalbard, Norway)	mineral				2			Westermann et al., 2009
Tundra (Svalbard, Norway)	organic	1.3			2.3			Westermann et al., 2009
Tundra (Svalbard, Norway)	snow pack	0.45			0.75			Westermann et al., 2009
Tundra (Northslope, Alaska)	West dock: peat (depth: 0-0.2)		1.2	0.6		1.26	2.7	Romanovsky & Osterkamp, 1997
Tundra (Northslope, Alaska)	Deadhorse: peat (depth: 0.0-0.12)		1.2	0.6		1.26	2.7	Romanovsky & Osterkamp, 1997
Tundra (Northslope, Alaska)	Franklin Bluffs: peat (depth: 0.0-0.08)		1.2	0.6		1.26	2.7	Romanovsky & Osterkamp, 1997
Soil (Manhattan, Kansas)	quartz	8.4			1.942			Peters-Lidard et al., 1998
Soil (Manhattan, Kansas)	mineral	2.9			1.942			Peters-Lidard et al., 1998
Soil (Manhattan, Kansas)	organic	0.25			2.503			Peters-Lidard et al., 1998
Soil (Manhattan, Kansas)	water	0.6			4.186			Peters-Lidard et al., 1998
Soil (Manhattan, Kansas)	ice	2.5			1.883			Peters-Lidard et al., 1998
Soil (Manhattan, Kansas)	air	0.026			0.0012			Peters-Lidard et al., 1998
Tundra (Northslope, Alaska)	organic/moss		0.1-0.7					Nicolsky, Romanovsky, & Tipenko, 2007
Tundra (Northslope, Alaska)	mineral/organic		0.9-1.6					Nicolsky, Romanovsky, & Tipenko, 2007
Tundra (Northslope, Alaska)	mineral		1.3-2.4					Nicolsky, Romanovsky, & Tipenko, 2007

It was determined that for the flux plate method, parameters measured by Hinzman et al. (1998) best represented the soils at Tiksi (values highlighted in Table 6 in green) due to the site descriptions and relative similar latitude of both study areas. Additionally, it was important to capture soil values collected in both frozen and thawed conditions, and Hinzman et al. (1998) was able to provide values for both conditions. In using soil property values from previous research, this study unfortunately cannot address variations in soil moisture on the soil parameters over both time and space. This is an obvious shortcoming that will introduce uncertainty in the storage change term.

The frozen and thawed state of the soils in Tiksi were defined by the presence or absence of snow at the station as snowy conditions signify freezing temperatures. The snow depth (or presence) data was obtained from manual observations collected daily by on-site technicians (Makshtas, 2017). The observed presence or absence of snow was compared against the calculated albedo from the observatory using the BSRN solar radiation measurements to verify the snowy conditions. The presence or absence of snow correlated directly with the albedo derived product calculated from the ratio of shortwave upwelling and downwelling solar radiation. It was identified that frozen soil time periods ranged from January 1^{st} – June 4^{th} and September 24th – December 31^{st} for the year 2016, with all other days of the year identified as thawed soil periods (Figure 8).

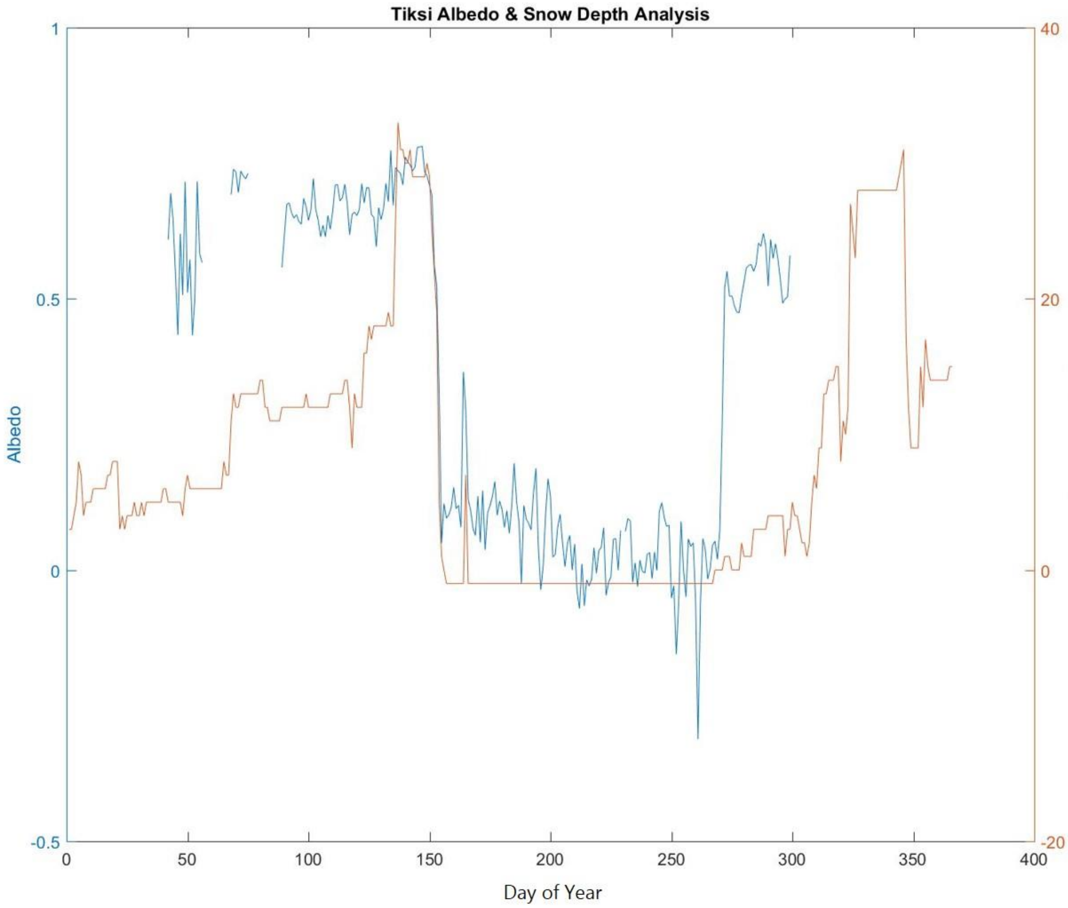

Figure 8. Annual cycle of snow depth and albedo collected from the Tiksi observatory in 2016. The radiation data used to calculate albedo was not quality controlled, so non-physical values of albedo exist briefly in later summer.

5. Results

5.1 Ground Heat Flux Variability

The full annual cycle of ground heat flux (Q_G), including the storage change term, at each of the five sub-sites is show in Figure 9.

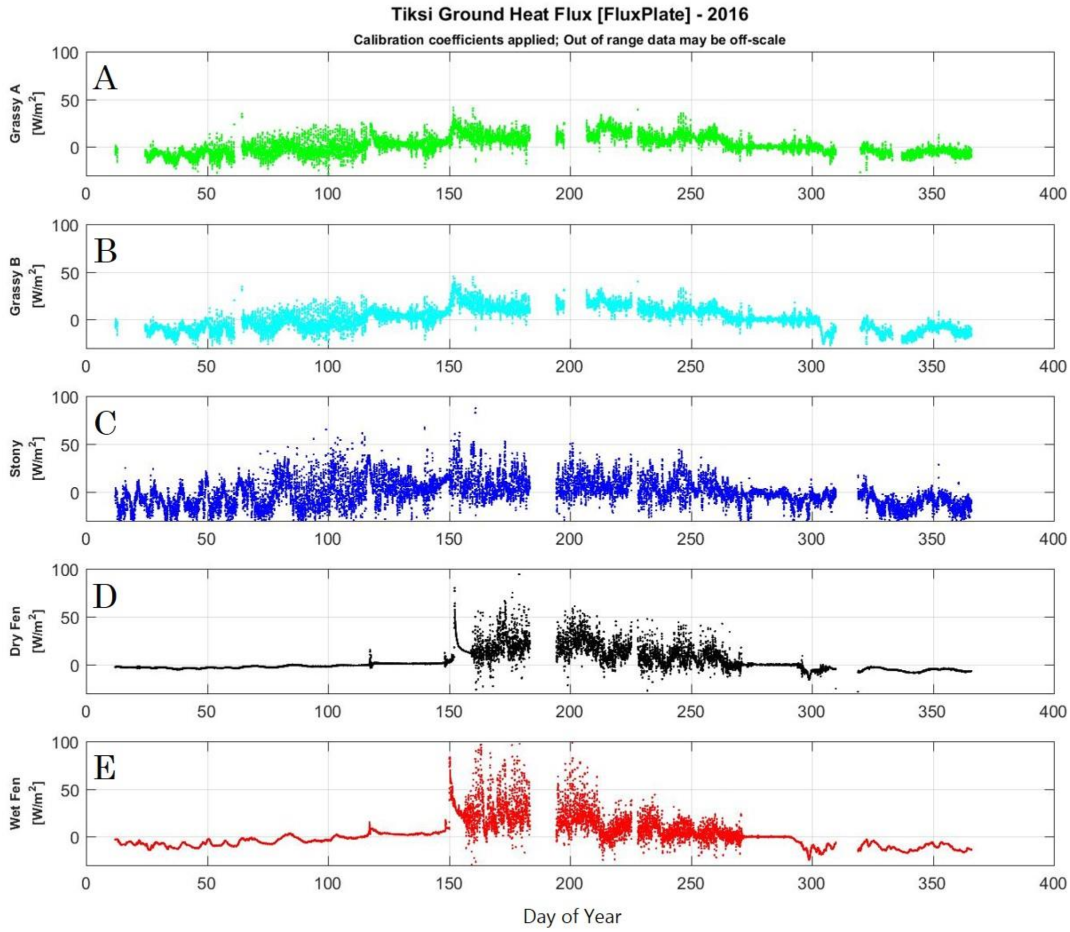

Figure 9. Annual cycle of the ground heat flux (Q_G) from all of the sub-station land cover types (panels **A-E** denote the land cover type). Note that GrassyA and GrassyB are both located in the Grassy land cover type, and are the only two flux plates co-located. Data gaps from power outages onsite occurred on DOY 0-12, DOY 183-194, DOY 226-228, and DOY 310-319.

Differences between the soil heat fluxes measured at each site are immediately apparent in Figure 9. Specifically, there is larger temporal variability at the Dry Fen and Wet Fen sites, compared to GrassyA, GrassyB, and Stony sites, in summer, while the opposite is true in winter. Note that the Stony site has the least amount of soil moisture than any of the sites, and Wet Fen has the most saturated soil. This variation between land cover types is likely due to differences in soil moisture content. Soil moisture is expected to be much higher in the saturated sites than the others, but this was not directly measured on-site and was only assessed qualitatively. From Figure 9 it is plausible that the spatial variability of the ground heat flux signal is large relative to the annual or temporal cycle variability in any one land cover type (Expectation 2-2).

It is clear that the ground heat flux in saturated soils is larger during the summer months compared to the grassy or dry/stony land cover types, with a smaller dampened signal during winter when water in the active layer has frozen (Figure 9). The temporal variability in Figure 9D and 9E during the summer months is larger than the variability of 9A, 9B, and 9C. During winter the ground heat flux in the saturated soils (Figure 9D and 9E) has a smaller dampened signal when water in the active layer has frozen. The stony/dry land cover type (Figure 9C) remains more constant over the annual cycle and does not appear to be as impacted by seasonality as the other sites. The ground heat fluxes at the grassy land cover type (Figure 9A and 9B) are not as variable as those at the saturated land cover types. However, they do show differences during the frozen and thawed months in that during winter, the values are primarily negative, while in the summer they are primarily positive. Therefore Expectation 1-1 is supported because soil moisture content does appear to impact the ground heat flux as shown by the variability in ground heat flux across the land covers. Similarly, the results from the annual ground heat flux measurements demonstrate that fluxes will attain small or negative values during winter months as the soils freeze, supporting Expectation 2-1.

Table 7 shows the calculated monthly, seasonal and annual means along with their standard deviations for ground heat flux at each of the land cover types.

Table 7. Monthly, annual and seasonal means for each land cover type. Area-weighted GHF was calculated by multiplying the flux values from each land cover type by its corresponding area and then dividing the summation of the weighted averages by the known area (Section 6.2). The summer season was defined as June 5th – September 23rd, with all other days of the year identified as the winter season. The land cover types are organized from least saturated (Stony) to most saturated (Wet Fen).

Land Cover Type	Monthly Means [W/m2] ± std											
	January	February	March	April	May	June	July	August	September	October	November	December
Stony	-9.7 ± 9.5	-11.01 ± 11	-2.5 ± 15.6	4.2 ± 18.1	7.02 ± 11.9	9.2 ± 15	9.2 ± 11.7	5.5 ± 10.6	0.8 ± 11.6	-5.6 ± 6.5	-9 ± 10.7	-12.5 ± 7.7
Grassy A	-6.8 ± 3.4	-8.3 ± 5.2	-1.9 ± 7	0.8 ± 9.1	4.6 ± 6.6	11.2 ± 6.2	12.8 ± 6.04	12.2. ± 6.3	7.2 ± 6.8	-0.3 ± 2.8	-5.4 ± 4.3	-6.06 ± 3.8
Grassy B	-8.6 ± 3.6	-11.02 ± 5.5	-3.05 ± 7.6	-0.06 ± 8.8	6.2 ± 8.2	15.2 ± 6.5	17.8 ± 4.9	12.1 ± 5.4	6.5 ± 6.3	-1.5 ± 5.6	-11.9 ± 5.7	-12.3 ± 5.5
Dry Fen	-2.9 ± 0.3	-3.7 ± 0.6	-1.9 ± 0.97	-0.7 ± 1.4	2.6 ± 7	18.9 ± 12.3	22.3 ± 11.5	10 ± 9.3	5.2 ± 8.4	-2.4 ± 3.6	-4.5 ± 1.7	-6.2 ± 1.4
Wet Fen	-7.5 ± 2.3	-9.02 ± 2.4	-3.7 ± 3.3	-0.5 ± 3.6	7.02 ± 12.2	27 ± 18.58	22.2 ± 16.2	7.4 ± 9.09	2.7 ± 6.3	-5.5 ± 6.9	-10 ± 3.8	-12 ± 3.3
Area-Weighted GHF	***-6.9 ± 3.2***	***-8.2 ± 3.6***	***-2.7 ± 5***	***0.7 ± 5.5***	***5.6 ± 7.5***	***18.5 ± 11.13***	***15.3 ± 8.6***	***8.4 ± 7.3***	***3.6 ± 6.7***	***-4 ± 4.3***	***-7.2 ± 3.6***	***-9.7 ± 3.3***

Table 7. Continued

Land Cover Type	Yearly Mean [W/m^2] ± std	Seasonal Mean [W/m^2] ± std	
		Summer DOY 157-267	Winter DOY 1-156 & 268-365
Stony	-1.02 ± 14.4	6.6 ± 12.1	-3.3 ± 13.8
Grassy A	1.9 ± 9.3	8.2 ± 7.3	-1.8 ± 7.6
Grassy B	1 ± 11.6	8.8 ± 7.5	-3.7 ± 10
Dry Fen	2.8 ± 10.7	14.2 ± 12.4	-1.01 ± 4.8
Wet Fen	1.5 ± 14.8	14.9 ± 17.1	-3.7 ± 6.4
Area-Weighted GHF	***1.2 ± 10.7***	***11.4 ± 10.3***	***-2.9 ± 7.6***

The seasonal means have a range of about 7 to 15 Wm^{-2} during summer months and about -4 to -1 Wm^{-2} during winter months. During the spring transition month of April, all of the land cover types (with the exception of the Stony land cover type) have a monthly mean of near-zero. In the fall transition month of October, there is a wide spread of variability, where only the GrassyA and GrassyB land cover types have values near-zero, suggesting a minimal transfer of energy or temperature gradient during that time. The two saturated land cover types (Dry Fen and Wet Fen) display the largest range in monthly means throughout the annual cycle, with monthly averages ranging from -6 to -12 Wm^{-2} in December and 19 to 27 Wm^{-2} in June.

Figure 10 further summarizes the variability across each land cover type for the full annual cycle organized by season.

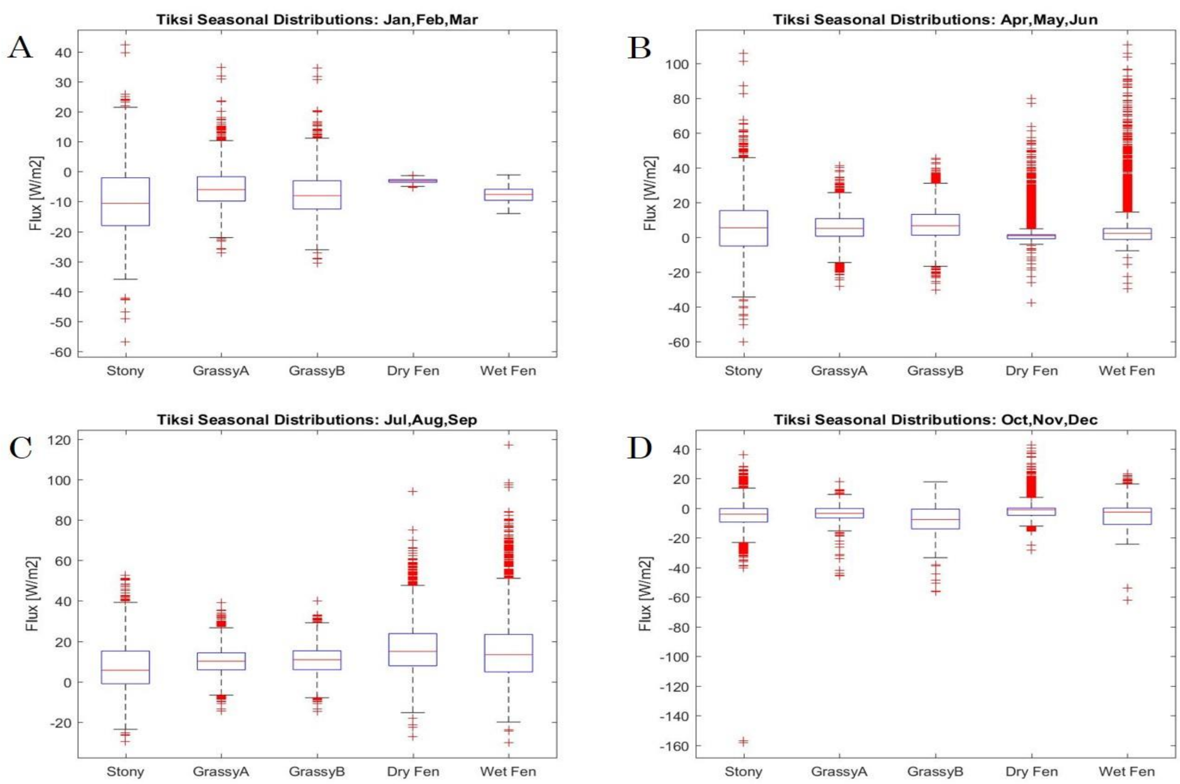

Figure 10. Box-and-whisker plots of the seasonal mean, standard deviation, and outliers of ground heat flux in each land cover type. Panel **A** shows monthly means for Jan-March, panel **B** shows monthly means for April – June, panel **C** shows monthly means for July – September, panel **D** shows monthly means for October – December.

The saturated sites, Wet Fen and Dry Fen, have a large number of outliers during the summer months, but very few during winter when the soil water has frozen. The Stony and Grassy [A, B] sites have the most outliers across the entire annual cycle. A 2-sample Kolmogorov-Smirnov (KS) test was used to compare the land cover types to one another, not making any assumptions about the distribution shape of the data. The KS-test shows that all of the data collected from the different land classes were significantly different from one another during the collected seasons, with p-values all less than a significance level of 0.05 (Table 8).

Table 8. Results from the 2-sample KS test showing a significant difference between the seasonal data collected from the different land classifications. All comparisons were statistically significant, with p-values < 0.05.

2-Sample Kolmogorov-Smirnov (KS) Test Results			
Seasons Compared	**Groups Compared**		***p-values (< 0.05)***
JFM	Stony	GrassyA	*1.81E-143*
		GrassyB	*2.47E-71*
		Dry Fen	*0*
		Wet Fen	*1.94E-234*
	GrassyA	GrassyB	*1.15E-30*
		Dry Fen	*0*
		Wet Fen	*5.60E-83*
	GrassyB	Dry Fen	*0*
		Wet Fen	*1.29E-66*
	Dry Fen	Wet Fen	*0*
AMJ	Stony	GrassyA	*3.90E-41*
		GrassyB	*9.31E-41*
		Dry Fen	*1.15E-286*
		Wet Fen	*2.35E-133*
	GrassyA	GrassyB	*1.12E-19*
		Dry Fen	*0*
		Wet Fen	*5.91E-157*
	GrassyB	Dry Fen	*0*
		Wet Fen	*2.01E-230*
	Dry Fen	Wet Fen	*1.29E-257*
JAS	Stony	GrassyA	*1.88E-109*
		GrassyB	*2.05E-110*
		Dry Fen	*4.70E-147*
		Wet Fen	*7.02E-81*
	GrassyA	GrassyB	*8.04E-06*
		Dry Fen	*1.61E-119*
		Wet Fen	*1.38E-83*
	GrassyB	Dry Fen	*1.26E-111*
		Wet Fen	*5.66E-87*
	Dry Fen	Wet Fen	*1.06E-11*
OND	Stony	GrassyA	*3.74E-47*
		GrassyB	*1.97E-66*
		Dry Fen	*1.83E-106*
		Wet Fen	*2.26E-41*
	GrassyA	GrassyB	*3.06E-191*
		Dry Fen	*1.96E-54*
		Wet Fen	*1.57E-73*
	GrassyB	Dry Fen	*0*
		Wet Fen	*4.74E-56*
	Dry Fen	Wet Fen	*5.89E-153*

Using a T-Test to test one could also compare if the ground heat flux results were statistically significant from zero. Results from T-Test's show that there is a significant difference between the seasonal data collected from each land classification and zero, with p-values < 0.05 (Table 9).

Table 9. Results from T-Test comparing each seasonal land classification to zero. All comparisons were statistically significant, with p-values < 0.05.

T-Test Comparison Against Zero		
Land Classification	**Season**	***p-values (< 0.05)***
Stony	JFM	*0*
	AMJ	*5.72E-118*
	JAS	*2.92E-230*
	OND	*8.51E-193*
GrassyA	JFM	*0*
	AMJ	*0*
	JAS	*0*
	OND	*0*
GrassyB	JFM	*0*
	AMJ	*0*
	JAS	*0*
	OND	*0*
Dry Fen	JFM	*0*
	AMJ	*1.38E-115*
	JAS	*0*
	OND	*3.28E-23*
Wet Fen	JFM	*0*
	AMJ	*2.35E-156*
	JAS	*0*
	OND	*5.80E-261*

In addition, further investigation of the saturated sites show that a phenomenon occurs from September 27th through October 19th where the ground heat fluxes remain steady at or near zero Wm^{-2} (Figure 11).

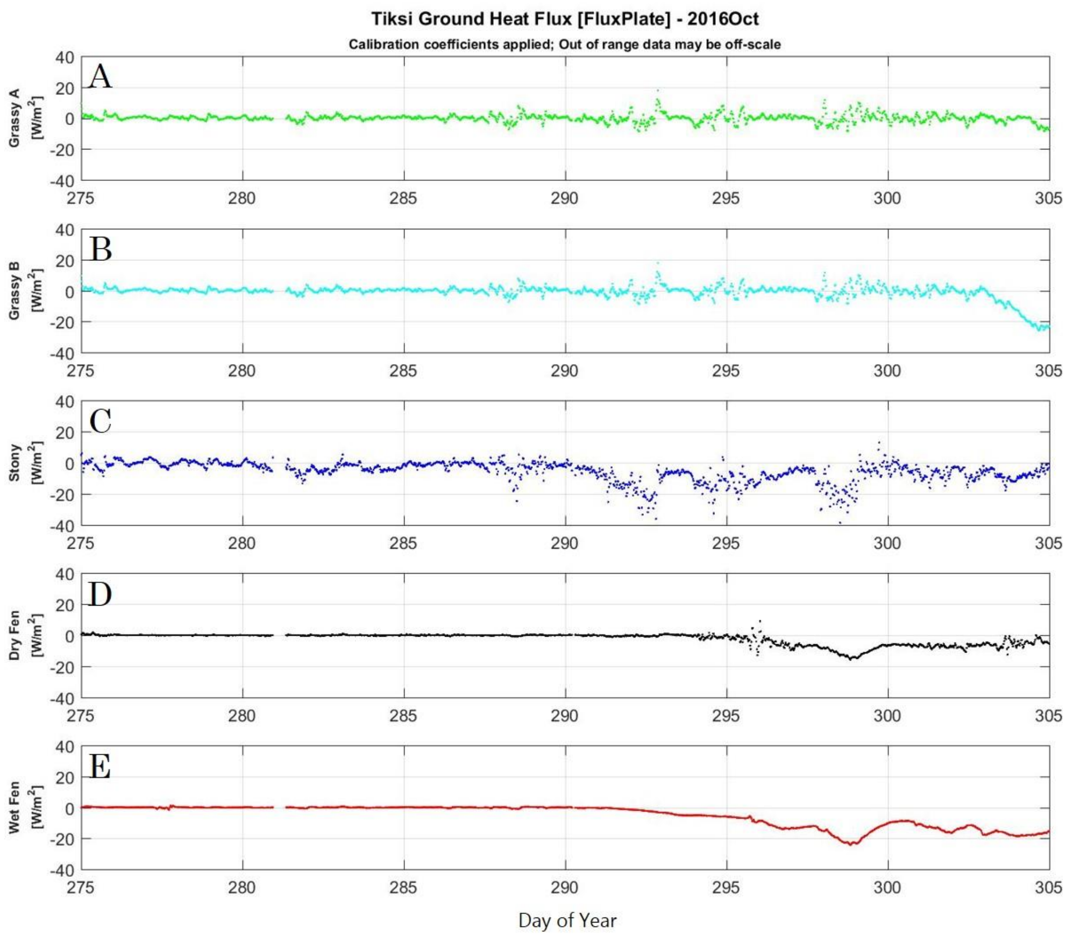

Figure 11. Demonstration of the zero-curtain effect that occurred at Tiksi in 2016 during the month of October whereby the ground heat flux (Q_G) becomes near-zero (panels **A-E** denote the land cover type).

This is known as the zero-curtain effect during which energy exchanges through the freezing soil are latent rather than thermal, resulting in a ground heat flux of zero for an extended period of time (Grachev et al., 2017; Outcalt, Nelson, & Hinkel, 1990). Meaning that because of the dramatic shift in turbulent heat flux during the transition from a warm summer season to fall, a continuous vertical temperature gradient of zero is seen in the ground heat flux (Grachev et al., 2017; Outcalt et al., 1990). These findings support Expectation 2-3 in that the saturated land cover types change abruptly during transition seasons, with the zero-curtain effect dominating during the autumn season.

By comparison, the regime shift in spring is abrupt (~DOY 150) and occurs over the course of only a week or two (Figure 9). This time period aligns with when the surface first becomes snow-free. This is also the time when the air temperature on-site increases rapidly from about -5 to +15°C. This shift is clear in the increase of the ground heat flux (Q_G) during the same time period as solar heating begins to influence the flux, as seen in Figure 9. Figure 12 shows the general meteorology (air temperature, relative humidity, solar radiation, and soil temperature) at Tiksi for the years 2014-2016 to show that there was little variability in the year 2016 from preceding years in relation to the measurements taken on-site.

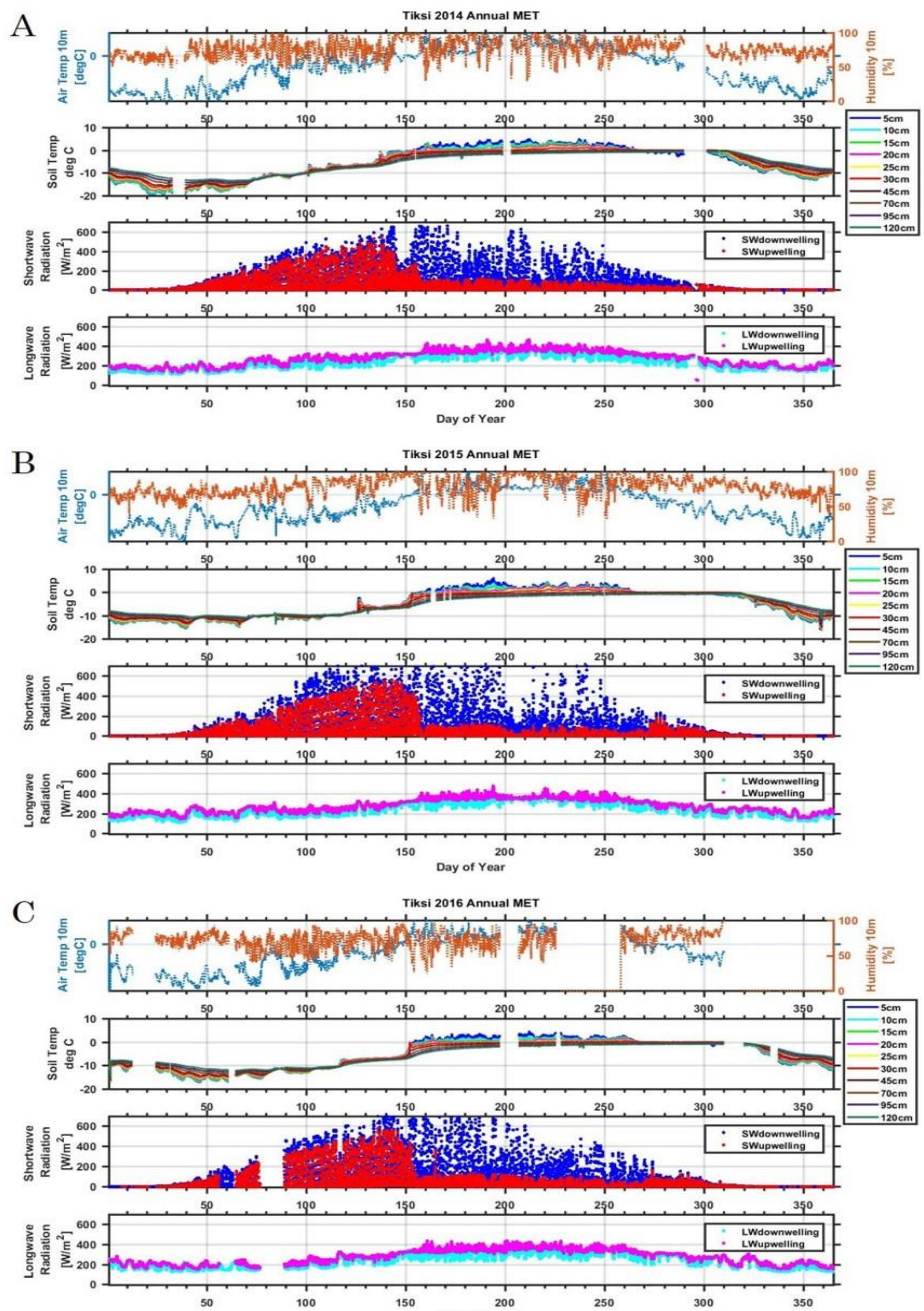

Figure 12. Panel's **A – C** show the meteorological conditions at Tiksi station for years 2014 (**A**), 2015 (**B**), and 2016 (**C**). In each panel for the years 2014-2016 are 10 meter air temperature and humidity, followed by upwelling and downwelling shortwave and longwave solar radiation. For 2016 Tiksi appears to have slightly less relative humidity with a cooler spring season, but in general there was little to no deviation from previous years.

5.2 Influence of Solar Forcing

To further assess the temporal variation in the data sets, the solar forcing was removed to understand its impact on the ground heat flux. This was done by calculating the solar zenith angle using the latitude, longitude, and altitude of the observatory. By then taking the cosine of the solar zenith angle (i.e. mu, μ), the ground heat flux could be plotted as a function of mu (μ) (Cox, 2017). With this information it was possible to derive an equation from the linear line of best fit of the distributions to quantify the solar forcing (Cox, 2017). This derived linear equation is then subtracted from the ground heat flux observation to remove the solar forcing signal. The derivation of the linear best fit excluded ground heat flux values during those times when the sun was below the horizon, taken as solar zenith angle (SZA) greater than 93 degrees, so that diffuse twilight was not included (Cox, 2017).

The scatter plot of ground heat flux (Q_G) plotted as a function of the cosine of the SZA revealed an interesting anomaly produced by the 30-minute averaging. Note the clustering of values (vertical stripes) that occur as a function of sun angle for values where the cosine of the SZA > 0.1 (Figure 13).

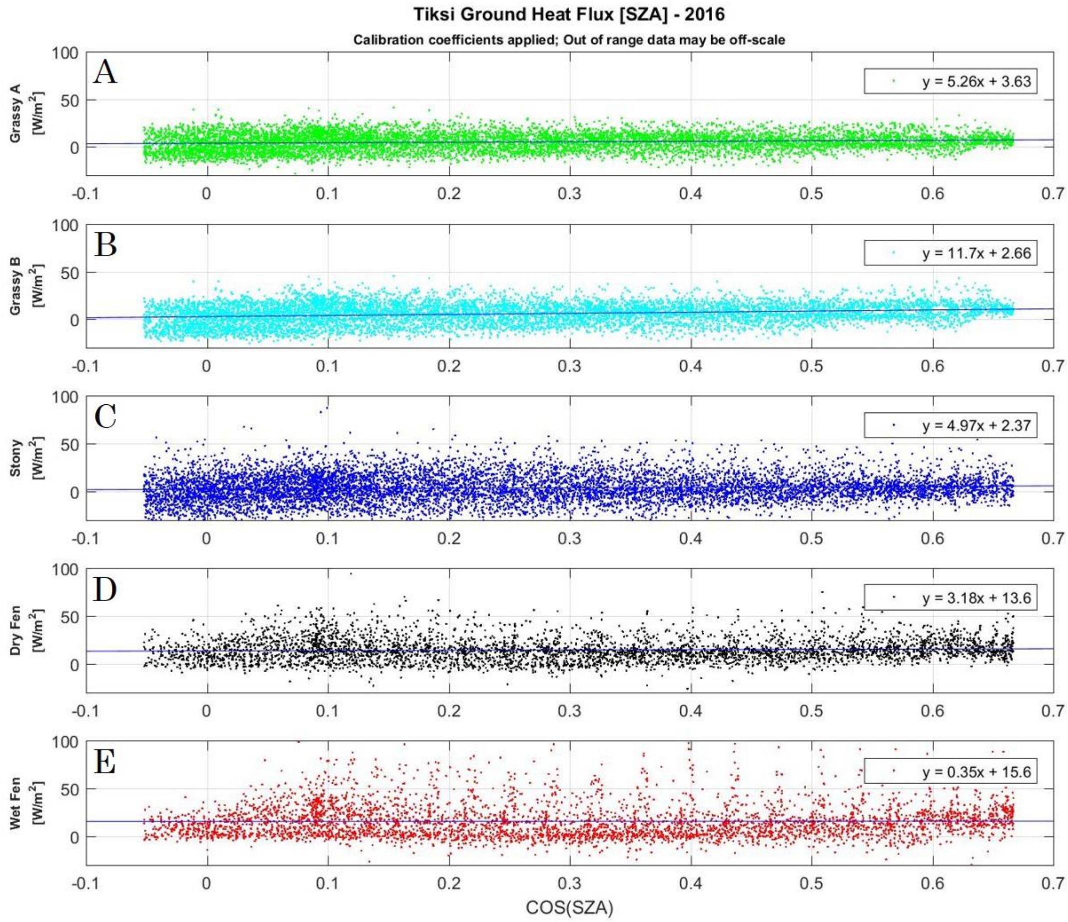

Figure 13. Panels **A – E** show the ground heat flux from each land cover classification as a function of the cosine of the SZA. Time periods during the year when the sun was below the horizon were excluded. Notice the clustering of oscillations as a result of the sampling frequency seen in **D** and **E**.

The source of the clustering was investigated by comparing the number of values that fall into bins of SZA from the 30-minute averages to those based on hourly averages. These differ by approximately a factor of two (Figure 14), suggesting the explanation of an oscillating pattern resulting from the sampling frequency (Cox, 2017).

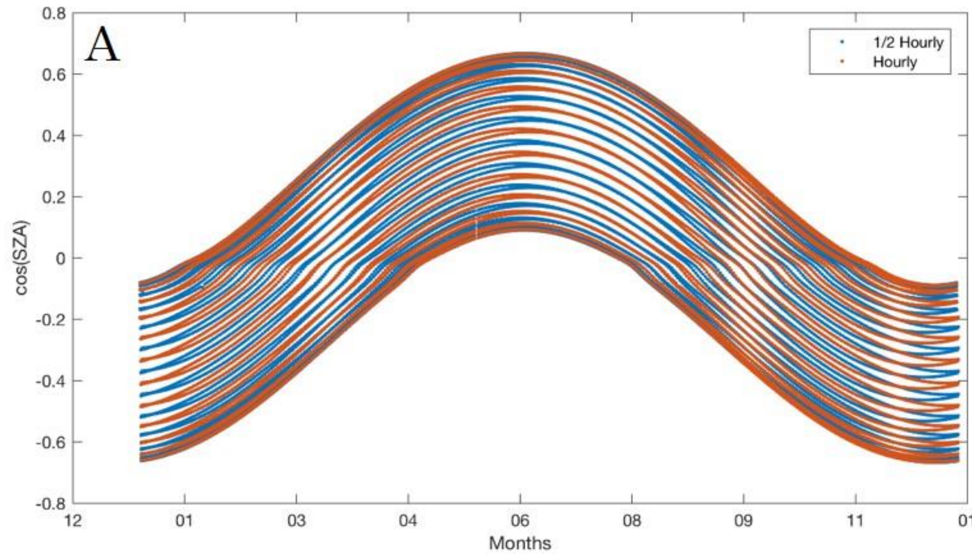

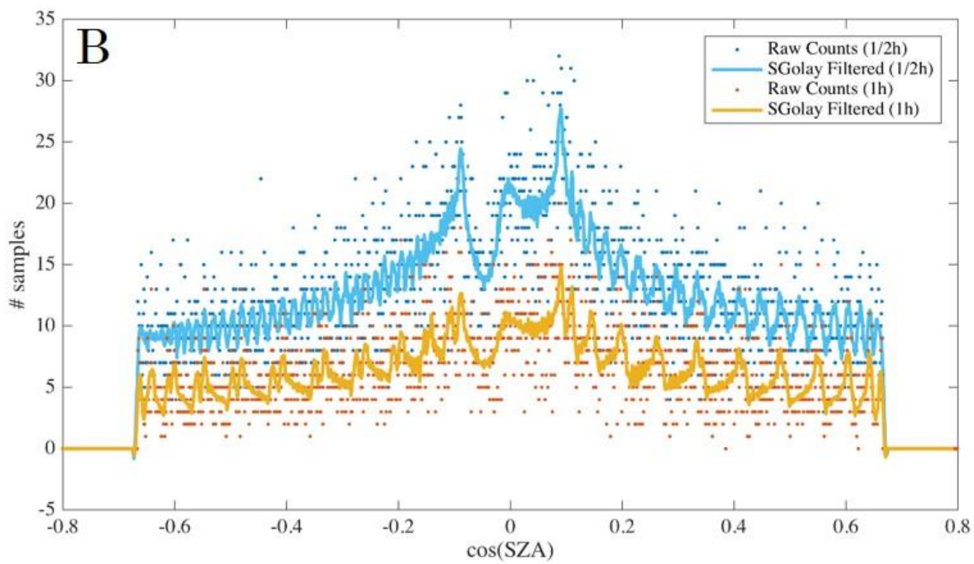

Figure 14. The top plot (**A**) shows the solar zenith angle over the course of the year. The blue lines utilize a half-hour sampling frequency and the orange lines utilize an hour sampling frequency. The bottom plot (**B**) shows the oscillations of the two sampling frequencies plotted via the cosine of the SZA.

These oscillations are not expected to impact the linear fit from which the linear equation is derived (Cox, 2017).

An analysis of the annual cycle of the ground heat flux was then conducted to assess the impact of the solar forcing on the measurement output. Figure 15 shows that there is considerable variability even when the solar forcing signal is removed using this method.

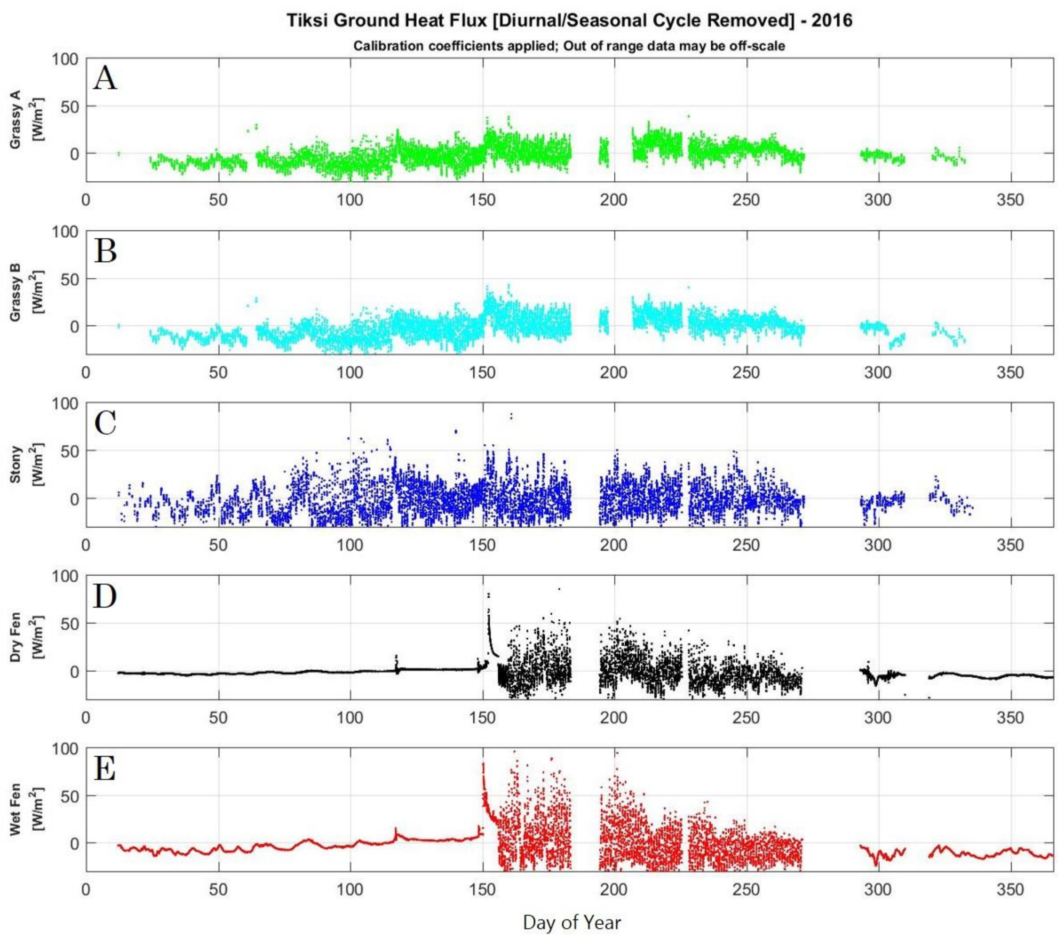

Figure 15. Annual ground heat flux values with the solar forcing signal removed (panels **A-E** denote the land cover type). The solar forcing was only removed for periods when the sun was above the horizon.

Table 10 shows the correlation coefficients between the original ground heat flux values and values after the solar forcing signal was removed; ~21-40% of the annual cycle in ground heat flux at Tiksi is linked to solar forcing.

Table 10. Results from correlation tests between ground heat flux values that include the solar forcing signal and those that do not. The variability in % to the far right shows the variability that can be accounted for in the signal due to the solar forcing.

Correlation Coefficients		r	p-values (<0.05)	r^2	Variability: $[1 - r^2] * 100$
[r1,p1] = corrcoef(wet_flux, wet_flux_de-trended)	R1	0.77	0	0.59	40.71%
[r2,p2] = corrcoef(mid_flux, mid_flux_de-trended)	R2	0.81	0	0.66	34.39%
[r3,p3] = corrcoef(dry_flux, dry_flux_de-trended)	R3	0.88	0	0.77	22.56%
[r4,p4] = corrcoef(twrA_flux, twrA_flux_de-trended)	R4	0.89	0	0.79	20.79%
[r4,p4] = corrcoef(twrB_flux, twrB_flux_de-trended)	R5	0.86	0	0.74	26.04%

Since this analysis was completed using a full annual cycle, the 21-40% variance explained is somewhat deceptive and would actually be much larger in summer and negligible in winter during polar-night.

Due to the variability still present in Figure 15 it was important to evaluate individual months when the sun was above the horizon to deduce if the solar forcing signal had actually been removed. Figure 16 shows ground heat flux values after the solar forcing signal has been removed for the month of August.

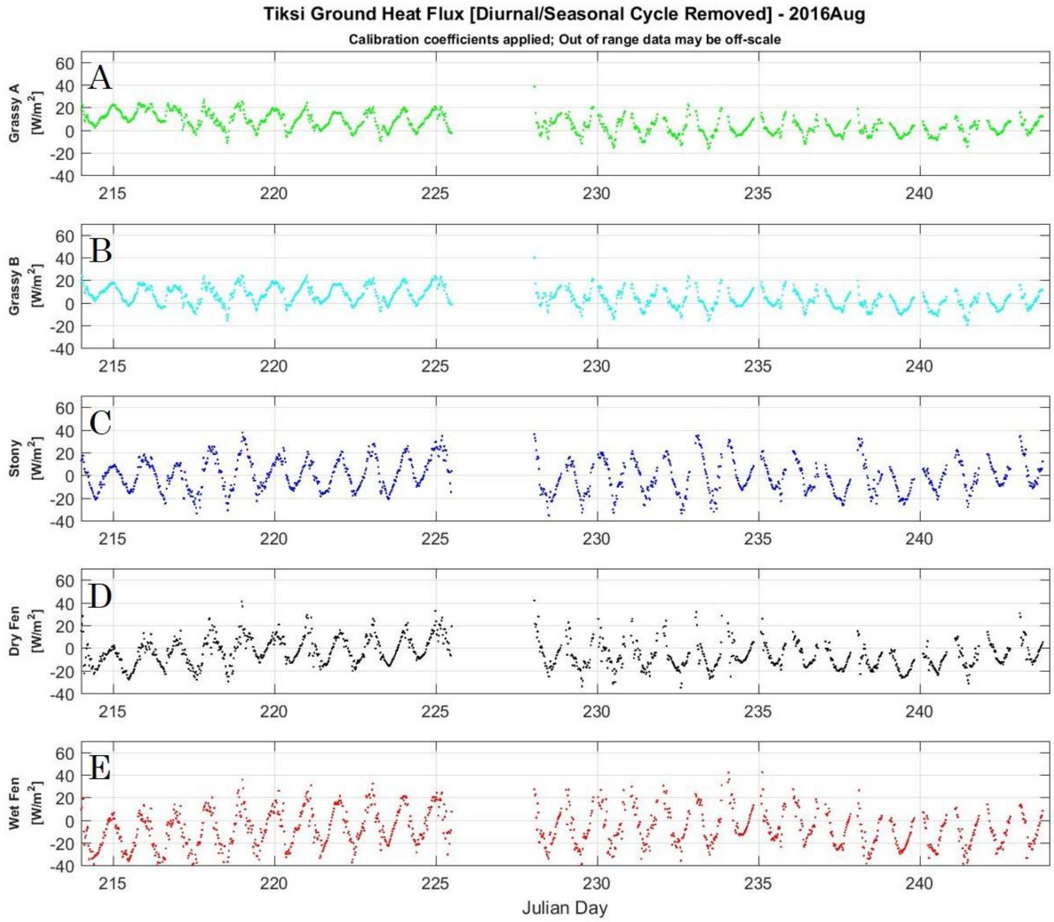

Figure 16. Ground heat flux (Q_G) for the month of August, after the solar forcing signal has been removed. It is apparent from the distinguishable cycles noted in all of the land cover types that the solar forcing signal was not completed removed using this method.

It is clear in Figure 16 that the solar forcing signal was unfortunately not completely removed from the ground heat flux, and that either a partial diurnal cycle or annual cycle still exists in the measurement. This could be due to the ground heat flux (Q_G) not being a direct function of the incoming solar radiation, but instead a function of surface temperature. Either way, it is revealed from Figure 16 that the solar forcing signal was not completely removed using this method.

5.3 Storage Change Term Influence

By comparing the flux output from the instrument to the storage change term it is seen that most of the signal noise is introduced by the storage change term on short time scales (i.e. 30-minute averages). Figure 17 shows the difference in the signal between the measured fluxes and the storage change values.

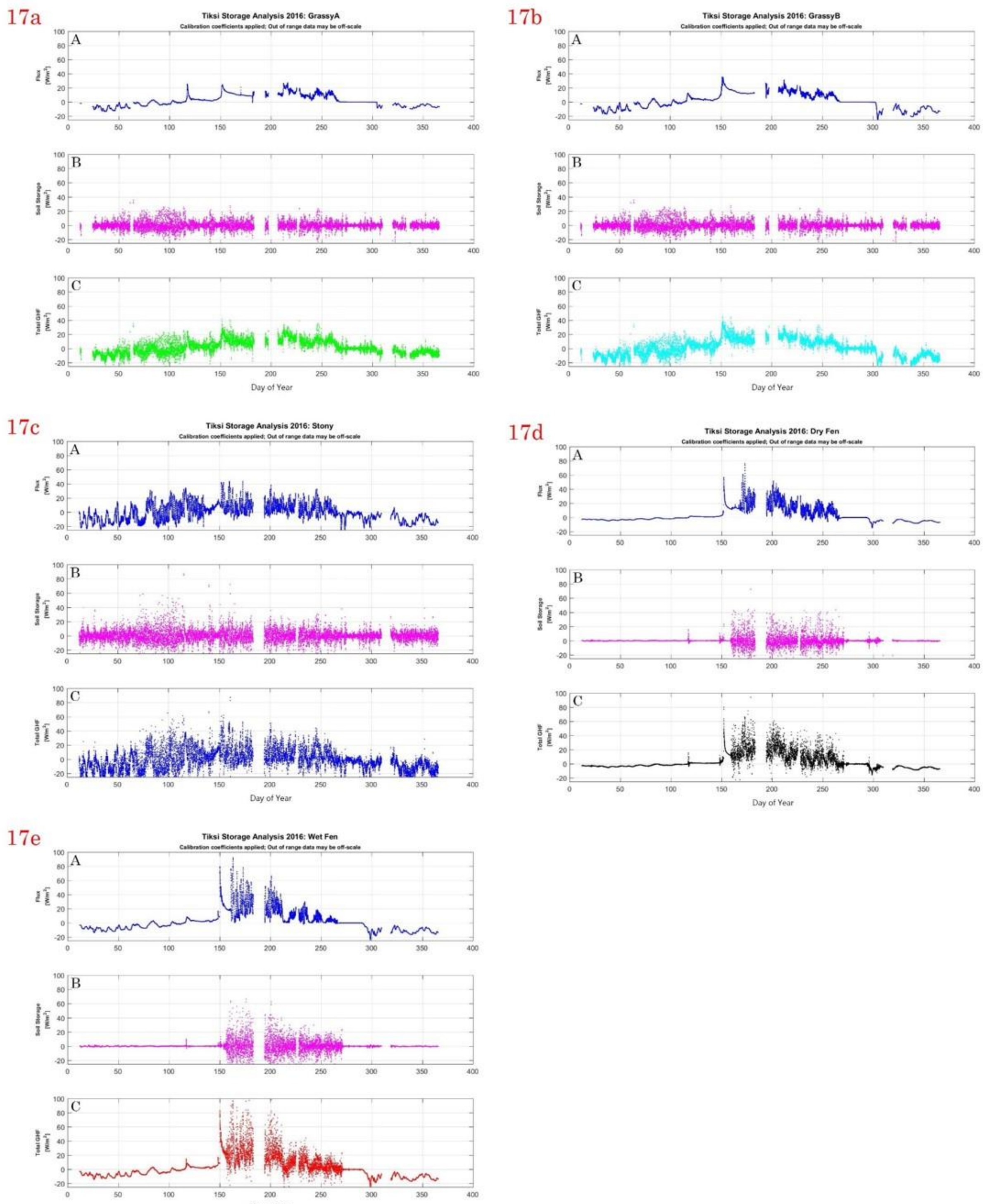

Figure 17. Comparison of the measured ground heat flux (G: in blue), the calculated storage change term (S: in pink), and the adjusted ground heat flux (Q_G) in the third sub-plot for each panel. Panel **17a** shows the GrassyA land cover, panel **17b** shows the GrassyB land cover, panel **17c** shows the Stony land cover, panel **17d** shows the Dry Fen land cover, and panel **17e** shows the Wet Fen land cover.

A closer look at the isolated storage change soil term (S) shows that it accounts for much of the variability of the total adjusted ground heat flux signal (Q_G) depending on land cover type and temperature/season for these 30-minute averages.

By investigating a series of running means of the adjusted ground heat flux (Q_G) one can investigate how averaging influences the significance of the storage term (S). Similarly, normalizing the running means by the sampling frequency of 30-minutes will show the percent decrease of the storage term over difference averaging periods. Figure 18 shows the influence of the storage term through investigation of running means from different averaging periods.

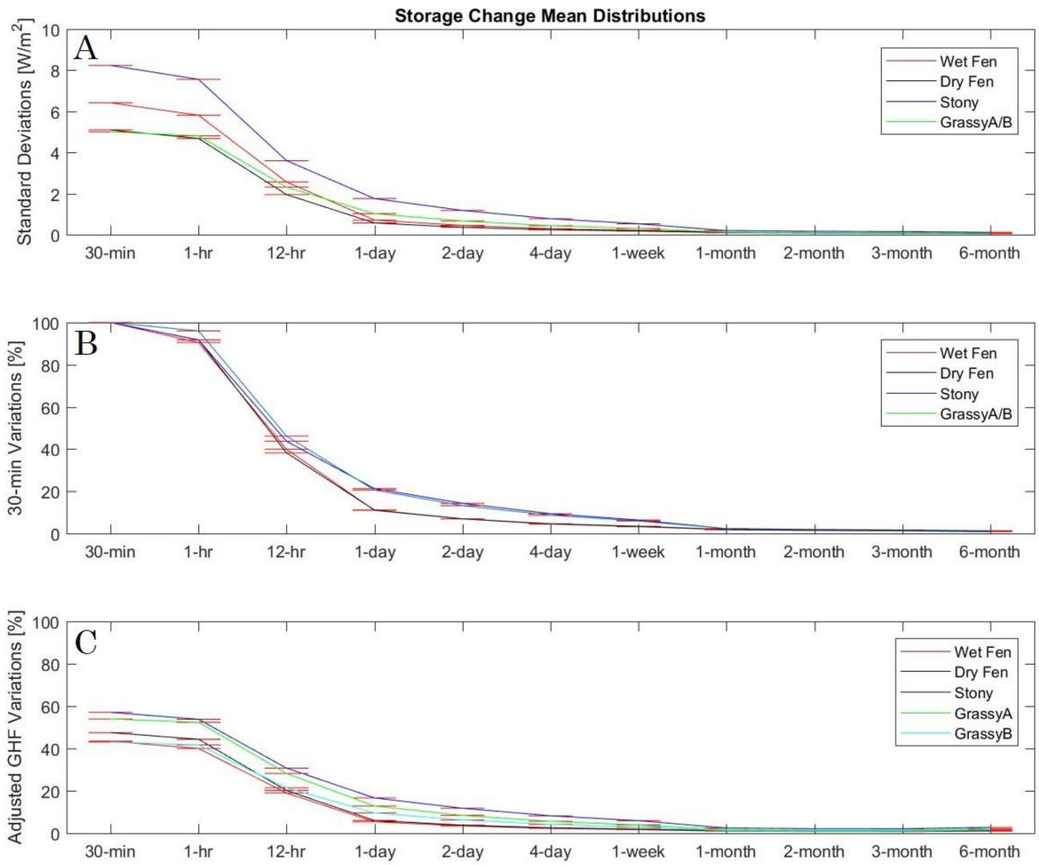

Figure 18. Panel **A** shows the standard deviations of different averaging periods for each of the land cover types. Panel **B** shows the percent variation of the storage term normalized by the initial 30-mintue collection frequency over different averaging periods for each land cover type. Panel **C** shows the percent variation of the storage change (S) relative to the variation of ground heat flux (Q_G) over different averaging periods for each land cover type.

The results from Figure 18A show how the standard deviation of the storage term (S) decreases as the averaging period increasing. This suggests that the storage term becomes negligible for longer averaging periods. Similarly, the results from Figure 18B show that by normalizing the storage term by the original 30-minute sampling frequency, longer averaging periods are less influenced by the storage term (S). Specifically, we can see that 1-day means show significant variations of 10 – 20% of the 30-minute variations, and that monthly means show a less significant variation. Figure 18C shows that the storage term (S) variation relative to the variation in ground heat flux (Q_G) accounts for almost 50% during shorter averaging periods, and almost 0% for averaging periods longer than 1-month.

Additionally, since the snowpack has the potential to store energy during the winter seasons (whether or not that energy influences the ground heat flux) it is worth investigating how much energy could be stored in the snow pack if it was included in the adjusted ground heat flux. It is found that including this term (when snow is present) further increase the variability in the adjusted ground heat flux (Figure 19).

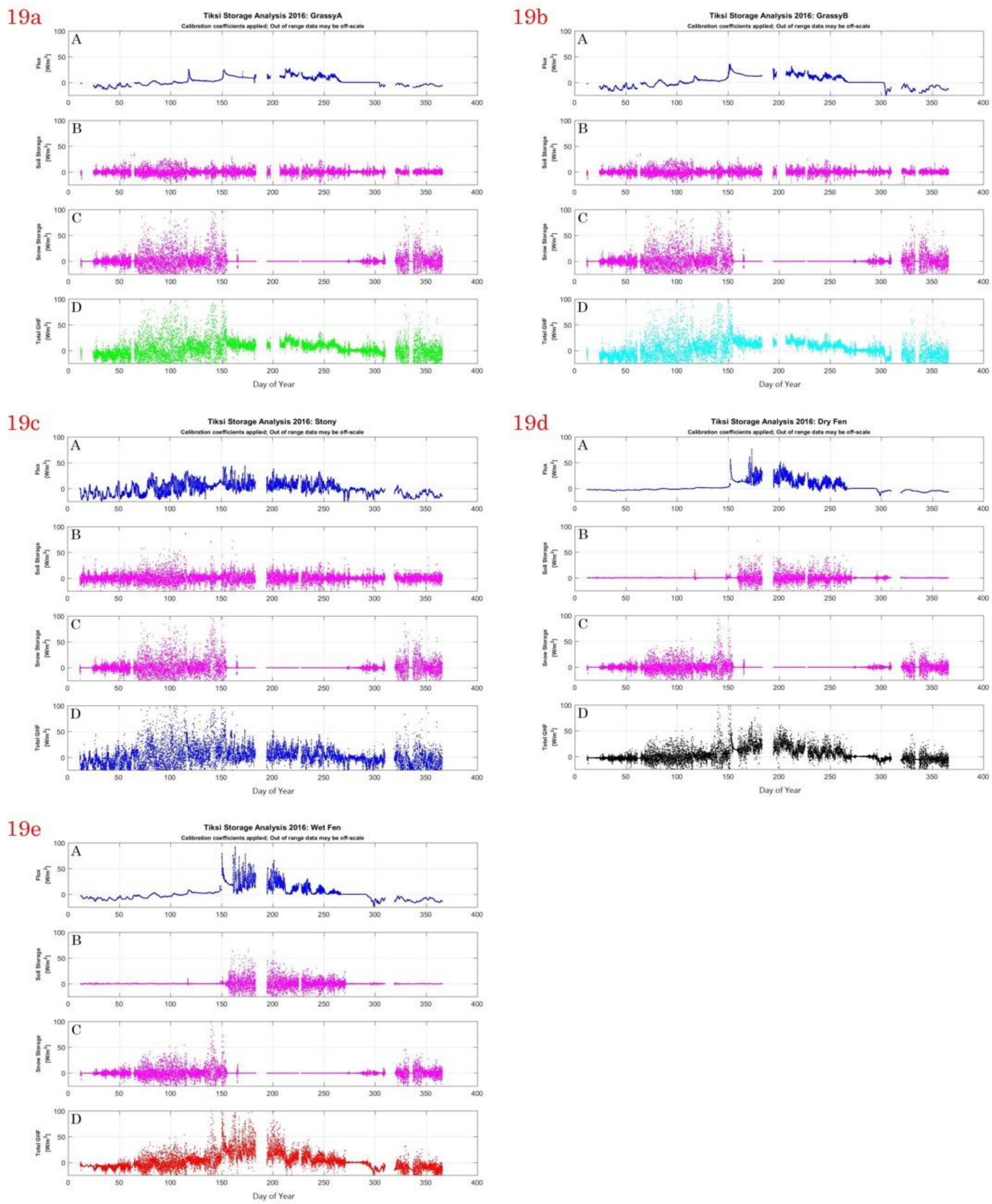

Figure 19. Comparison of the measured ground heat flux (in blue), the adjusted storage change term in the soil (second sub-plot), the storage change in the snow pack (third sub-plot), and the adjusted ground heat flux (fourth sub-plot) for each panel. Panel **19a** shows the GrassyA land cover, panel **19b** shows the GrassyB land cover, panel **19c** shows the Stony land cover, panel **19d** shows the Dry Fen land cover, and panel **19e** shows the Wet Fen land cover.

The storage of energy from the snow pack was not included in the final (adjusted) ground heat flux term (Q_G) since the skin temperature term was defined as the interface between the soil and atmosphere. The depth of the snow pack was determined by daily measurements from an on-site technician and the heat capacity of snow-pack was based on values reported by Westermann et al. (2009) from Table 6. The temperature above the snow pack was measured from the infrared Apogee sensor, and the temperature below the snow pack was measured from the Nokeval sensors located at the Stony, Dry Fen, and Wet Fen sites (for the Grassy location the Stony Nokeval data was used for temperatures below the snow pack). Overall, the resulting storage change snow term (S_{snow}), when coupled with the traditional storage change soil term (S) and ground heat flux measurement, increased the variability of the final flux output during the winter seasons when snow was present (Figure 19). This increased variability could be due to differences in the snow pack, which would be expected to dampen the temporal variation (N. B. Miller et al., 2017).

Because soil properties (soil heat capacity and thermal conductivity) were not directly measured, it is instructive to plot a range of ground heat flux values using ranges of soil property values. Figure 20 shows the resulting ground heat flux ranges.

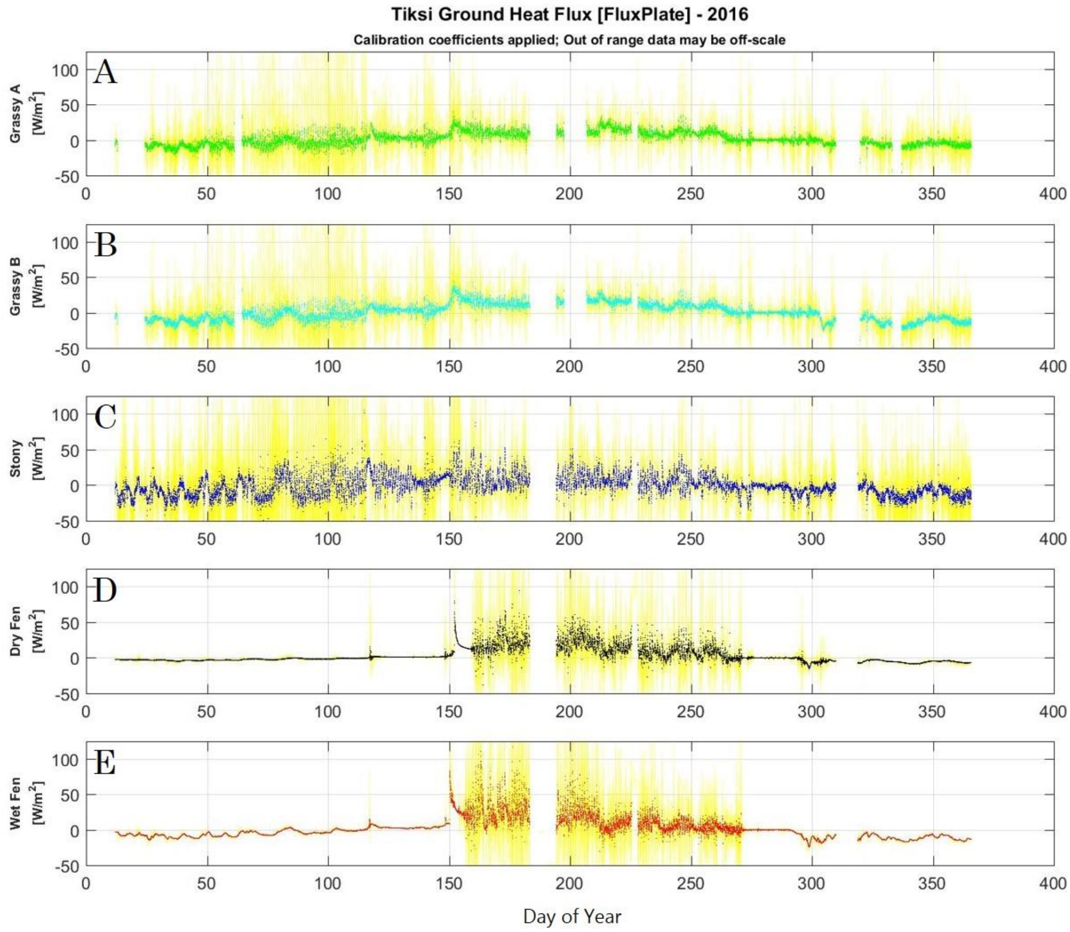

Figure 20. Ground heat fluxes as seen in Figure 9 along with values based on a range of soil properties (in yellow).

The range in soil properties were based on results by Hinzman et al. (1998) for Barren soil types on the North slope of Alaska and Water soil types from the same location. This range, shown in Figure 20, essentially spans the storage change situation of soils that are dry with no vegetation to soils that are submerged in water.

6. Discussion: Improving Measurements

6.1 Instrument Influence

The influence of the ground heat flux instrumentation stems from both instrument biases and instrument specifications. Flux plate biases were derived from a comparison between the two sensors (A & B) positioned in the Grassy land cover type. Since these two sensors were the only ones located in a similar land cover type, they are the only ones that could be compared directly. The comparison of these two instruments is based on root-mean-square (RMS) differences and a comparison of squared correlations. Results follow in Table 11.

Table 11. Comparisons between results from flux plates (G) at each the GrassyA and Grassy B locations to evaluate how the instruments compare to one another. This comparison is most useful when instruments are co-located, so the results from the comparison of GrassyA and GrassyB are most accurate (compared to the other sub-station instruments) to determine instrument biases. Error was determined by instrument specifications, while biases were determined by instrument comparison. The RMS difference was smaller than the annual mean.

Measurement Type	Comparison	r^2	RMS Difference [W/m^2]	Instrument Error (30-minute)	Bias
Ground Heat Flux	GrassyA / GrassyB	0.92	3.9	± 3 - 8 % [± 1 - 4 W/m^2]	± 4 W/m^2

Note that the comparison in Table 11 is from the flux plate outputs only (G) and does not include the storage change term.

There is a 3.9 Wm^{-2} difference (or ~4 Wm^{-2} instrument bias) between the two flux plates (A & B) located in the Grassy land cover type, assuming no difference in soil properties within the Grassy land classification. It did not make sense to compare flux plates from the other land cover types because one could not isolate the instrument uncertainty from the spatial variability of the different land cover types. The final comparison of the r-squared values also suggests that output from the two instruments closely agree ($r^2 = 0.92$).

The instrument manual from the Hukseflux manufacturer of the flux plates was also evaluated. The specifications note that the factory calibration of the instruments include a calibration uncertainty of ± 3%. The manufacturer also cites that uncertainty will increase by <1% for each year of operation in the field. The two flux plates located in the Grassy land cover type were installed in the spring of 2011 and have not been re-calibrated since installation, meaning that uncertainty for the year 2016 could be ± 5%. In addition to the ± 3% calibration uncertainty, the operation uncertainty of ± 5% results in a total uncertainty of ± 8% or about 1 – 4 Wm^{-2}, not including the 4 Wm^{-2} instrument bias.

The uncertainty analysis for this study only included flux plate outputs (G) – larger uncertainties likely exist in the other terms used to obtain the storage change term (and could be investigated in future research). However, from the results of the instrument analysis, it is concluded that one can indeed anticipate that the ground heat flux at Tiksi is large enough to be measured by available tools, supporting Expectation 3-1, not including the impact of soil moisture properties. Additionally, the method used to measure the ground heat flux can impact uncertainty. Since the flux plate method measures the thermal gradient across a known material, unlike the thermistor temperature probe approach that utilizes soil temperature gradients, the flux plate method introduces less error to the observation.

6.2 Weighted Average Ground Heat Flux

Tiksi provides a unique opportunity to assess how ground heat flux varies across the landscape by utilizing the five flux plates currently on-site. Most other Arctic sites only collect data from a single flux plate, which is used to quantify ground heat flux for the entire region. One potential solution to deriving the most representative flux of a region is to weight each known ground heat flux (Q_G) according to its land cover type area. By taking the area details from Table 2 one can then weight the known ground heat flux in the vicinity of the station using the dimensions specified. Figure 21 highlights in white the area of the map where ground heat flux can be accounted for, the remaining area is in black.

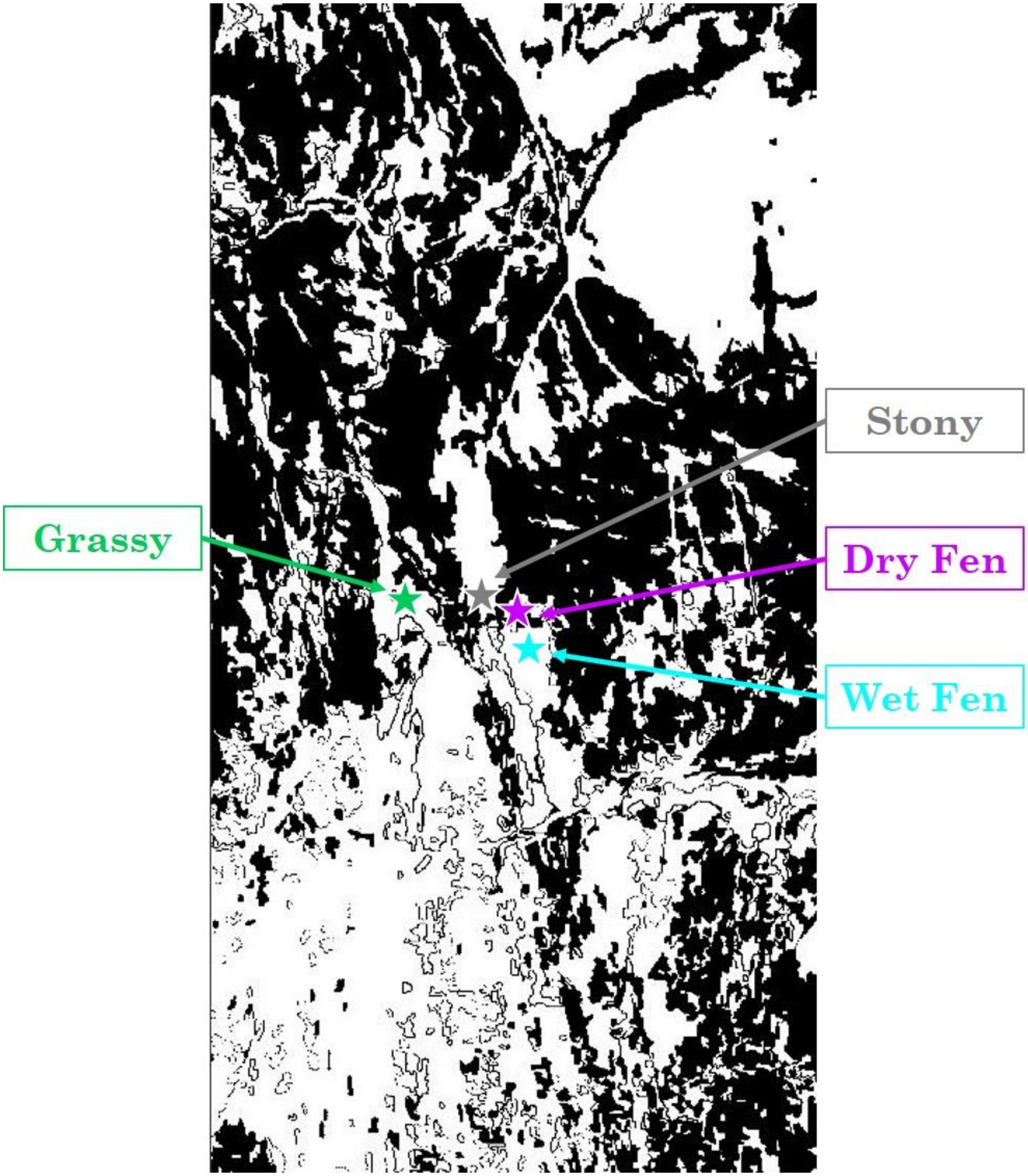

Figure 21. Area map of Tiksi observatory created by Mikola et al. (2018). Areas highlighted in white are land cover types where the ground heat flux was measured while areas highlighted in black are areas where flux was not measured. White = 49% of the total image, Black = 51% of the total image.

The area-weighted ground heat flux was calculated by multiplying the flux values from each land cover type by its corresponding area and then dividing the summation of the weighted averages by the known area. Since there are two represented flux plates in the Grassy land cover type, only GrassyA was included in the summation and not GrassyB so that the Grassy area was not duplicated. The area-weighted flux is plotted against each land cover type flux in Figure 22.

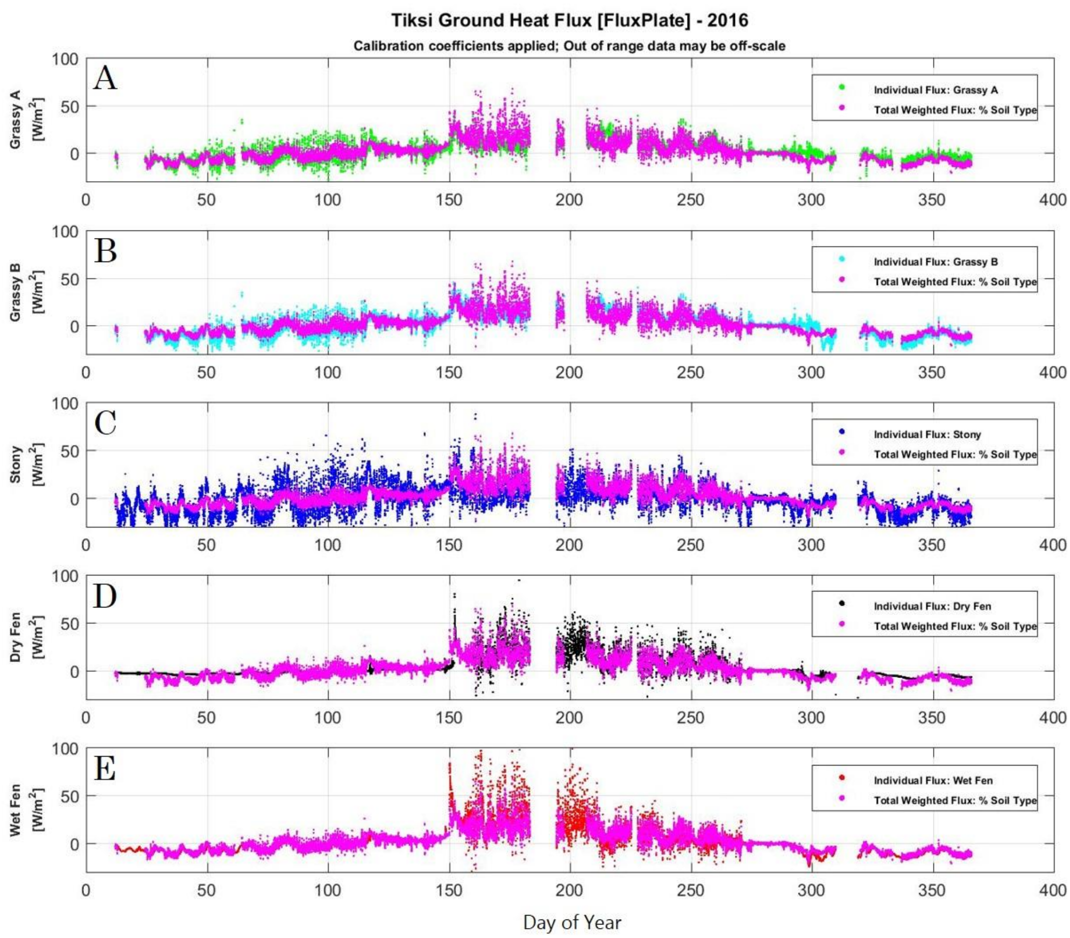

Figure 22. Ground heat flux (Q_G) values for each land cover type plotted with the calculated area-weighted ground heat flux (in pink). Area-weighted ground heat flux is calculated by multiplying the flux values from each land cover type by its corresponding area and then dividing the summation of the weighted averages by the known area.

It is seen that the area-weighted flux (in pink) has much less variability than the flux at the individual sites. This weighting method may be particularly useful to the modeling community in that model grid cell resolution does not allow for such small-scale details to be included. By instead capturing the area-weighted average ground heat flux of a vicinity or region, modelers can better compare modeled ground heat flux against direct observations, with the caveat of needing to know or map land cover type areas in the region. A potential issue with this approach, however, is in justifying the area size domain to the user; the area-weighted ground heat flux value will change depending on how the area is defined.

Comparing against the means from Table 7, it seems that the saturated sites over-estimate the regional summer seasonal and annual means, while under-estimating the regional winter seasonal mean. The Stony site appears to under-estimate the annual and winter regional means and over-estimate the means in summer. The Grassy A and B fluxes both over-estimate the summer seasonal and annual means, while under-estimating the winter seasonal mean. It is concluded that, in line with Expectation 1-2, a more representative regional ground heat flux can be calculated using the area-weighted average of the fluxes measured in the different land cover types found in the vicinity, but more will need to be done to determine the best way to define the area or domain size needed for a weighted flux average.

7. *Conclusion*

7.1 *Re-defining Ground Heat Flux Calculations*

Variability in the ground heat flux (Q_G) around the Tiksi observatory is strongly related to land cover type. It is clear that it is insufficient to measure ground heat flux at only one location in an environment such as Tiksi. The results show that for short time scales (30-minutes or less), ground heat flux can vary by as much as ~20 Wm^{-2} depending on land cover type. This leads to the conclusion that we should re-define how and where ground heat flux is measured in the Arctic. Careful consideration must be given to the spatial distribution of the measurements. A single site-specific ground heat flux is not a good regional estimate; the flux needs to be representative of the more general environment, meaning that measurements need to be made at multiple points across a site. Of the factors that impact a ground heat flux measurement, the soil and moisture content is key, but the types of instruments used can also play a role (i.e. flux plate, thermistor, infrared skin temperature sensor, etc.).

Traditionally, for longer time scales only the ground heat flux output (G) has been collected with no inclusion of a storage change term (S) to reflect energy gained or lost in the soil layer directly above the flux plate. In part, this has reflected shortcomings in instrumentation and infrastructure (Foken, 2008). With increasing infrastructure support and improved instrument technology, the community now has the opportunity to capture parameters like soil moisture content while also mapping landscapes in remote locations to investigate impacts of the storage change term (S) on ground heat flux. Results showed that the storage change term (S) can account for almost half of the adjusted ground heat flux value (Q_G) (Figure 17), meaning that by not including it in the adjusted ground heat flux, one is underrepresenting the term's impact on the overall surface energy budget for time scales less than 1-day (Foken, 2008).

Additionally, ground heat flux measurements and observations can be improved if soil moisture content is captured spatially using tools like World View-2 or other satellite mapping techniques. Understanding that the ground heat flux is influenced by soil moisture (which can be assumed using vegetation characteristics), it is important to capture the measurement in each type of soil present in the vicinity being quantified. This was shown in the area-weighted ground heat flux results (Table 7, Figure 22) where the weighted results were better able to quantify the regional ground heat flux. Using satellite mapping techniques, one should be able to identify the types of soil or land cover present in a region and utilize this information to guide where to install flux plates. Flux plates are relatively inexpensive, so it is cost-effective to invest in outfitting stations with multiple sensors at different locations.

7.2 Overview of Results

In general, the results from the study concluded that it is possible to measure the ground heat flux in the Arctic with reasonable accuracy. However, methods used could be improved upon by 1) including proper soil moisture measurements in the same vicinity as the flux measurements, 2) characterizing the land cover types in the region, and 3) adopting an area-weighted approach for determining ground heat flux. The flux plate instrument currently used at several Arctic locations provides a more accurate output than the method based on thermistor temperature probes since the flux plate design utilizes a known heat capacity for the temperature gradient to be measured across.

It was found that the zero-curtain effect was most prominent in ground heat flux observations collected in saturated land cover types, where ground heat flux values remain at near-zero values during the summer to fall transition season. This is thought to be the result of a continuous vertical temperature gradient of zero from a latent heat exchange that is reflected in the ground heat flux measurement (Grachev et al., 2017; Outcalt et al., 1990). Additionally, the spring transition of ground heat flux was abrupt, reflecting the rapid transition from snow-covered to snow-free conditions due to the sun returning from polar-night and solar radiation thereby beginning to warm the surface. Fluxes from the Stony land cover type, that contained little to no soil moisture, remained much more consistent throughout the annual cycle with winter season values being primarily negative (upward) and summer season values being primarily positive (downward).

Measured fluxes were similar to ranges reported in previous work, however the majority of those studies utilized a minimal suite of flux instruments (Grachev et al., 2017; N. B. Miller et al., 2017; Persson et al., 2002). Seasonal averages exhibit a range of ± 7 – 15 Wm^{-2} during summer months when the ground is thawed and frozen winter months show a range of ± -4 to -1 Wm^{-2}. The area-weighed ground heat flux seasonal averages displayed a summer value of ± 11.4 Wm^{-2} and a winter value of ± -2.9 Wm^{-2}. Solar forcing accounted for 21 – 40% of the variance in the ground heat flux signal, but it was later determined that the method used to remove solar forcing was not adequate in removing all of the solar forcing signal. An investigation of the storage change term (S) showed that the term becomes less important as the averaging period increases. Meaning that the storage term does not need to be included in averaging periods larger than 1-month.

The results from this study support previous work (Foken, 2008) suggesting that ground heat flux is a significant term, that if not properly accounted for, can contribute to errors in closing the surface energy budget. An analysis of the annual averages of the surface energy budget terms (Q^*, Q_E, Q_H, and Q_G) for 2016 at Tiksi shows that ground heat flux accounts for only ~5% of the surface energy budget. Though this small percentage may be insignificant or within the measurement errors of the surface energy budget, this small amount of energy produced by the ground heat flux can impact Arctic processes such as permafrost melt (Hinzman et al., 1991; Jacobsen, 1999). The sensitivity of the active layer and permafrost lends these small energy transfers, like that of the ground heat flux, to have large impacts on soil moisture melt (Romanovsky & Osterkamp, 1997). To further assess the influence of ground heat flux on Arctic soils, it is recommended that future studies make use of flux plates installed in all major land cover types in the vicinity.

Visualization tools such as satellite mapping will help determine where to position flux plates and to also determine the quantity of flux plates needed.

References

Apogee. (2015). SI-111: Standard Field of View Infrared Radiometer Sensor. Retrieved from http://www.apogeeinstruments.com/standard-field-of-view-infrared-radiometer-sensor-si-111/

Aurela, M. (2017a, 11/21/17). [Ground heat flux map].

Aurela, M. (2017b, 7/31/17). [Ground heat flux publication/thesis].

Blanken, P. (2015, 2/6/15). [Surface Flux Measurement Question].

Bloomfield, P. (1976). *Fourier Analysis of Time Series: An Introduction*. New York: John Wiley & Sons.

Boike, J., & Roth, K. (1997). Time domain reflectometry as a field method for measuring water content and soil water electrical conductivity at a continuous permafrost site. *Permafrost and Periglacial Processes, 8*(4), 359-370. doi:10.1002/(sici)1099-1530(199710/12)8:4<359::aid-ppp261>3.0.co;2-s

Boike, J., Roth, K., & Ippisch, O. (2003). Seasonal snow cover on frozen ground: Energy balance calculations of a permafrost site near Ny-Alesund, Spitsbergen. *Journal of Geophysical Research-Atmospheres, 108*(D1), 11. doi:10.1029/2001jd000939

Bristow, K. L. (2002). 5.3 Thermal Conductivity. In J. H. Dane & C. G. Topp (Eds.), *Methods of Soil Analysis: Part 4 Physical Methods*. Madison, WI: Soil Science Society of America.

Cable, W. L. (2010). Model of soil freezing and thawing. Retrieved from http://permafrost.gi.alaska.edu/content/model-soil-freezing-and-thawing

Callaghan, T. V., Johansson, M., Brown, R. D., Groisman, P. Y., Labba, N., Radionov, V., . . . Yang, D. (2011). The Changing Face of Arctic Snow Cover: A Synthesis of Observed and Projected Changes. *AMBIO, 40*(1), 17-31. doi:10.1007/s13280-011-0212-y

Carson, J. E. (1963). Analysis of soil and air temperatures by Fourier techniques. *Journal of Geophysical Research, 68*(8), 2217-2232. doi:10.1029/JZ068i008p02217

Cox, C. J. (2017, 12/20/17). [The Tiksi solar zenith angle problem].

Dozier, J., & Warren, S. G. (1982). Effect of viewing angle on the infrared brightness temperature of snow. *Water Resources Research, 18*(5), 1424-1434. doi:doi:10.1029/WR018i005p01424

Eaton, A. K., Rouse, W. R., Lafleur, P. M., Marsh, P., & Blanken, P. D. (2001). Surface energy balance of the western and central Canadian subarctic: Variations in the energy balance among five major terrain types. *Journal of Climate, 14*(17), 3692-3703. doi:10.1175/1520-0442(2001)014<3692:Sebotw>2.0.Co;2

ECMWF. (2004). Part IV: Physical Processes *IFS Documentation CY28R1*: ECMWF.

Eugster, W., Rouse, W. R., Pielke, R. A., McFadden, J. P., Baldocchi, D. D., Kittel, T. G. F., . . . Chambers, S. (2000). Land-atmosphere energy exchange in Arctic tundra and boreal forest: available data and feedbacks to climate. *Global Change Biology, 6*, 84-115. doi:10.1046/j.1365-2486.2000.06015.x

Evett, S. R., Agam, N., Kustas, W. P., Colaizzi, P. D., & Schwartz, R. C. (2012). Soil profile method for soil thermal diffusivity, conductivity and heat flux: Comparison to soil heat flux plates. *Advances in Water Resources, 50*, 41-54. doi:http://dx.doi.org/10.1016/j.advwatres.2012.04.012

Farouki, O. T. (1981). *Thermal Properties of Soils* (CRREL Monograph 81-1). Retrieved from U.S. Army Cold Regions Research and Engineering Laboratory: http://www.eng.usf.edu/~gmullins/downloads/Thermal/Thermal%20Properties%20of%20Soils.pdf

Foken, T. (2008). The energy balance closure problem: an overview. *Ecol Appl, 18*(6), 1351-1367. doi:10.1890/06-0922.1

Grachev, A. A., Persson, P. O. G., Uttal, T., Akish, E. A., Cox, C. J., Morris, S. M., . . . Repina, I. A. (2017). Seasonal and latitudinal variations of surface fluxes at two Arctic terrestrial sites. *Climate Dynamics*. doi:10.1007/s00382-017-3983-4

Halliwell, D. H., & Rouse, W. R. (1987). Soil Heat-Flux in Permafrost - Characteristics and Accuracy of Measurement. *Journal of Climatology, 7*(6), 571-584. doi:http://dx.doi.org/10.1002/joc.3370070605

Halliwell, D. H., Rouse, W. R., & Weick, E. J. (1991). *Surface Energy Balance and Ground Heat Flux in Organic Permafrost Terrain under Variable Moisture Conditions*. Paper presented at the Permafrost: Fifth Canadian Proceedings, Quebec City.

Helgason, W., & Pomeroy, J. (2012). Problems Closing the Energy Balance over a Homogeneous Snow Cover during Midwinter. *Journal of Hydrometeorology, 13*(2), 557-572. doi:10.1175/jhm-d-11-0135.1

Heusinkveld, B. G., Jacobs, A. F. G., Holtslag, A. A. M., & Berkowicz, S. M. (2004). Surface energy balance closure in an arid region: role of soil heat flux. *Agricultural and Forest Meteorology, 122*(1-2), 21-37. doi:10.1016/j.agrformet.2003.09.005

Hinkel, K. M. (1997). Estimating seasonal values of thermal diffusivity in thawed and frozen soils using temperature time series. *Cold Regions Science and Technology, 26*(1), 1-15. doi:http://dx.doi.org/10.1016/S0165-232X(97)00004-9

Hinzman, L. D., Goering, D. J., & Kane, D. L. (1998). A distributed thermal model for calculating soil temperature profiles and depth of thaw in permafrost regions. *Journal of Geophysical Research-Atmospheres, 103*(D22), 28975-28991. doi:10.1029/98jd01731

Hinzman, L. D., Kane, D. L., Gieck, R. E., & Everett, K. R. (1991). Hydrologic and Thermal-Properties of the Active Layer in the Alaskan Arctic. *Cold Regions Science and Technology, 19*(2), 95-110. doi:10.1016/0165-232x(91)90001-W

Hukseflux. (2015). HFP01 Heat Flux Sensor. Retrieved from http://www.hukseflux.usa.com/HFP01.php?pSection=heatFlux

IASOA. (2015). Tiksi, Russia: Observatory. Retrieved from http://www.esrl.noaa.gov/psd/iasoa/stations/tiksi

Jacobsen, A. (1999). Estimation of the soil heat flux/net radiation ratio based on spectral vegetation indexes in high-latitude Arctic areas. *International Journal of Remote Sensing, 20*(2), 445-461. doi:10.1080/014311699213532

Kane, D. L., Hinkel, K. M., Goering, D. J., Hinzman, L. D., & Outcalt, S. I. (2001). Non-conductive heat transfer associated with frozen soils. *Global and Planetary Change, 29*(3-4), 275-292. doi:10.1016/s0921-8181(01)00095-9

Koren, V., Smith, M., Cui, Z., Cosgrove, B. (2007). *Physically-Based Modifications to the Sacramento Soil Moisture Accounting Model: Modeling the Effects of Frozen Ground on the Rainfall-Runoff Process*. Retrieved from U.S. Department of Commerce: http://www.nws.noaa.gov/oh/hrl/hsmb/docs/hydrology/PBE_SAC-SMA/NOAA_Technical_Report_NWS_52.pdf

Kustas, W. P., Prueger, J. H., Hatfield, J. L., Ramalingam, K., & Hipps, L. E. (2000). Variability in soil heat flux from a mesquite dune site. *Agricultural and Forest Meteorology, 103*(3), 249-264. doi:https://doi.org/10.1016/S0168-1923(00)00131-3

Laurila, T. (2015, 9/4/15). [Soil heat fluxes].

Liebethal, C., Huwe, B., & Foken, T. (2005). Sensitivity analysis for two ground heat flux calculation approaches. *Agricultural and Forest Meteorology, 132*(3-4), 253-262. doi:10.1016/j.agrformet.2005.08.001

Makshtas, A. (2017). Archive of Tiksi standard meteorological observations (1932-2016). Retrieved from http://www.aari.ru/resources/d0024/archive/description_e.html

Masseroni, D., Corbari, C., & Mancini, M. (2014). Limitations and improvements of the energy balance closure with reference to experimental data measured over a maize field. *Atmosfera, 27*(4), 335-352. doi:10.1016/s0187-6236(14)70033-5

Meyers, T. P., & Hollinger, S. E. (2004). An assessment of storage terms in the surface energy balance of maize and soybean. *Agricultural and Forest Meteorology, 125*(1-2), 105-115. doi:10.1016/j.agrformet.2004.03.001

Mikola, J., Virtanen, T., Linkosalmi, M., Vähä, E., Nyman, J., Postanogova, O., . . . Aurela, M. (2018). Spatial variation and linkages of soil and vegetation in the Siberian Arctic tundra – coupling field observations with remote sensing data. *Biogeosciences Discuss., 2018*, 1-33. doi:10.5194/bg-2017-569

Miller, N. B., Shupe, M. D., Cox, C. J., Noone, D., Persson, P. O. G., & Steffen, K. (2017). Surface energy budget responses to radiative forcing at Summit, Greenland. *The Cryosphere, 11*(1), 497-516. doi:10.5194/tc-11-497-2017

Miller, N. B., Shupe, M. D., Cox, C. J., Walden, V. P., Turner, D. D., & Steffen, K. (2015). Cloud Radiative Forcing at Summit, Greenland. *Journal of Climate, 28*(15), 6267-6280. doi:doi:10.1175/JCLI-D-15-0076.1

MRC. (2015). Retrieved from ftp://ftp1.esrl.noaa.gov/psd3/arctic/tiksi/surface_properties/fluxtower/towermet/0_docs/MRC%20TP-100%202006_Temp_Probe_Flier.pdf

Muskett, R. R., Romanovsky, Vladimir E., Cable, William L., Kholodov, Alexander L. (2015). Active-Layer Soil Moisture Content Regional Variations in Alaska and Russia by Ground-Based and Satellite-Based Methods, 2002 through 2014. *International Journal of Geosciences, 6*(1), 12-41. doi:10.4236/ijg.2015.61002

Nicolsky, D. J., Romanovsky, V. E., & Panteleev, G. G. (2009). Estimation of soil thermal properties using in-situ temperature measurements in the active layer and permafrost. *Cold Regions Science and Technology, 55*(1), 120-129. doi:10.1016/j.coldregions.2008.03.003

Nicolsky, D. J., Romanovsky, V. E., & Tipenko, G. S. (2007). Using in-situ temperature measurements to estimate saturated soil thermal properties by solving a sequence of optimization problems. *The Cryosphere, 1*(1), 41-58. doi:10.5194/tc-1-41-2007

Nokeval. (2015). Retrieved from http://www.nokeval.com/index.php?language=english

Oliphant, A. J., Grimmond, C. S. B., Zutter, H. N., Schmid, H. P., Su, H. B., Scott, S. L., . . . Ehman, J. (2004). Heat storage and energy balance fluxes for a temperate deciduous forest. *Agricultural and Forest Meteorology, 126*(3-4), 185-201. doi:10.1016/j.agrformet.2004.07.003

Outcalt, S. I., Nelson, F. E., & Hinkel, K. M. (1990). The zero-curtain effect: Heat and mass transfer across an isothermal region in freezing soil. *Water Resources Research, 26*(7), 1509-1516. doi:10.1029/WR026i007p01509

Persson, P. O. G., Fairall, C. W., Andreas, E. L., Guest, P. S., & Perovich, D. K. (2002). Measurements near the Atmospheric Surface Flux Group tower at SHEBA: Near-surface conditions and surface energy budget. *Journal of Geophysical Research, 107*(C10). doi:10.1029/2000jc000705

Peters-Lidard, C. D., Blackburn, E., Liang, X., & Wood, E. F. (1998). The effect of soil thermal conductivity parameterization on surface energy fluxes and temperatures. *Journal of the Atmospheric Sciences, 55*(7), 1209-1224. doi:10.1175/1520-0469(1998)055<1209:Teostc>2.0.Co;2

Philip, J. R. (1961). The theory of heat flux meters. *Journal of Geophysical Research, 66*(2), 571-579. doi:10.1029/JZ066i002p00571

Putkonen, J. (1998). Soil thermal properties and heat transfer processes near Ny-Alesund, northwestern Spitsbergen, Svalbard. *Polar Research, 17*(2), 165-179. doi:10.3402/polar.v17i2.6617

Romanovsky, V. E., & Osterkamp, T. E. (1997). Thawing of the active layer on the coastal plain of the Alaskan Arctic. *Permafrost and Periglacial Processes, 8*(1), 1-22. doi:http://dx.doi.org/10.1002/(SICI)1099-1530(199701)8:1<1::AID-PPP243>3.0.CO;2-U

Rouse, W. R., Eaton, A. K., Petrone, R. M., Boudreau, L. D., Marsh, P., & Griffis, T. J. (2003). Seasonality in the surface energy balance of tundra in the lower Mackenzie River basin. *Journal of Hydrometeorology, 4*(4), 673-679. doi:Doi 10.1175/1525-7541(2003)004<0673:Sitseb>2.0.Co;2

Sari, J., Tarmo, V., Vladimir, K., Tuomas, L., Maiju, L., Juha, M., . . . Mika, A. (2017). Spatial variation and seasonal dynamics of leaf-area index in the arctic tundra-implications for linking ground observations and satellite images. *Environmental Research Letters, 12*(9), 095002.

Sellers, W. D. (1965). Heat Transfer in Soil *Physical Climatology* (pp. 127-133). Chicago: University of Chicago Press.

Serreze, M. C., & Barry, R. G. (2005). *The Arctic Climate System*. New York: Cambridge University Press.

Topp, G. C., Davis, J. L., & Annan, A. P. (1980). Electromagnetic determination of soil water content: Measurements in coaxial transmission lines. *Water Resources Research, 16*(3), 574-582. doi:10.1029/WR016i003p00574

Uttal, T., Makshtas, A., Laurila, T. (2013). The Tiksi International Hydrometeorological Observatory - An Arctic Members Partnership (Vol. 1). World Meteorological Organization.

Wang, Z. H., & Bou-Zeid, E. (2012). A novel approach for the estimation of soil ground heat flux. *Agricultural and Forest Meteorology, 154*, 214-221. doi:10.1016/j.agrformet.2011.12.001

Watanabe, K., Kiyosawa, H., Fukumura, K., Ezaki, T., & Mizoguchi, M. (2003). *Spatial and temporal variation in thaw depth in Siberian tundra near Tiksi.* Paper presented at the Permafrost, Vols 1 and 2, Leiden.

Westermann, S., Luers, J., Langer, M., Piel, K., & Boike, J. (2009). The annual surface energy budget of a high-arctic permafrost site on Svalbard, Norway. *Cryosphere, 3*(2), 245-263.

Yoshikawa, K., Overduin, P. P., & Harden, J. W. (2004). Moisture content measurements of moss (Sphagnum spp.) using commercial sensors. *Permafrost and Periglacial Processes, 15*(4), 309-318. doi:10.1002/ppp.505

Zhang, T., & Osterkamp, T. E. (1995). Considerations in determining thermal diffusivity from temperature time series using finite difference methods. *Cold Regions Science and Technology, 23*(4), 333-341. doi:http://dx.doi.org/10.1016/0165-232X(94)00021-O